Y3.At7
22/IDO-16314

IDO-16314
Physics
(TID-4500, 12th Ed.)

204

MTR TECHNICAL BRANCH QUARTERLY REPORT
THIRD QUARTER

Edited by W. P. Conner

November 1, 1956

AEC RESEARCH AND DEVELOPMENT REPORT

UNIVERSITY OF ARIZONA LIBRARY
Documents Collection
APR 1 1958

PHILLIPS PETROLEUM CO.
ATOMIC ENERGY DIVISION
(UNDER CONTRACT NO. AT (10-1)-205)
IDAHO OPERATIONS OFFICE
U.S. ATOMIC ENERGY COMMISSION

metadc67273

PRICE 45 ¢

Available from the
Office of Technical Services
U. S. Department of Commerce
Washington 25, D. C.

LEGAL NOTICE

This report was prepared as an account of Government sponsored work. Neither the United States, nor the Commission, nor any person acting on behalf of the Commission:

A. Makes any warranty or representation, express or implied, with respect to the accuracy, completeness, or usefulness of the information contained in this report, or that the use of any information, apparatus, method, or process disclosed in this report may not infringe privately owned rights; or

B. Assumes any liabilities with respect to the use of, or for damages resulting from the use of any information, apparatus, method, or process disclosed in this report.

As used in the above, "person acting on behalf of the Commission" includes any employee or contractor of the Commission to the extent that such employee or contractor prepares, handles or distributes, or provides access to, any information pursuant to his employment or contract with the Commission.

TABLE OF CONTENTS

LIST OF FIGURES

Previous Reports:

IDO-16094 First Quarter 1953
IDO-16117 Second Quarter 1953
IDO-16134 Third Quarter 1953
IDO-16153 Fourth Quarter 1953

IDO-16181 First Quarter 1954
IDO-16191 Second Quarter 1954
IDO-16209 Third Quarter 1954
IDO-16219 Fourth Quarter 1954

IDO-16229 First Quarter 1955
IDO-16235 Second Quarter 1955
IDO-16254 Third Quarter 1955
IDO-16259 Fourth Quarter 1955

IDO-16291 First Quarter 1956
IDO-16297 Second Quarter 1956

MTR TECHNICAL BRANCH QUARTERLY REPORT
Third Quarter - 1956

Edited by - W. P. Conner - Technical Director

Work Directed by - J. E. Evans, Section Chief Cross Sections
D. R. deBoisblanc, Section Chief Applied Physics & Instrumentation
H. L. McMurry, Section Chief Theoretical Physics
G. H. Hanson, Section Chief Special Engineering Studies

I. SUMMARY

In the course of the technical assistance to the overall operation of the MTR, two items of special interest were uncovered. An MTR fuel plate was seriously deformed at 10 percent over pressure during a hydraulic flow test of a standard fuel assembly. The deformation was traced to faulty fabrication in which about 11 inches of the fuel plate was improperly brazed to the side plates. Secondly, it now appears that the most likely source of the low level alpha contamination in the process water arises from a uranium impurity in the beryllium reflector.

With reference to the supporting facilities operated by MTR Technical, it is of interest to note that the IBM computing equipment is now loaded to capacity (one shift), there being no standby time. The improvement in the rigidity of the RMF now provides reactivity measurements having a standard deviation of $3 \times 10^{-6} \Delta k/k$. The pile oscillator, now being installed, should improve this sensitivity by a factor of 10 to 100.

In reactor physics, the conceptual designs of two reactors have been completed. A nuclear duplicate of the ETR, the ETR Critical Facility, will provide a means for measuring the reactivity effects and the flux distortion caused by the major ETR experiments without encroaching on valuable reactor time. A proposal has been submitted to the Commission for a Shielding Experiments Reactor which will supply large irradiation facilities for examining the behavior of massive components to fast fluxes on the order of 10^{11} neutrons/sq cm/sec and for carrying out shielding experiments in high fast and thermal neutron fluxes and gamma fields. A program is also under way to evaluate the performance of 20% enriched uranium as a fuel for high flux reactors. Exploratory calculations have been made to establish the maximum thermal neutron flux which can be realized in a testing reactor limited only by the maximum heat fluxes now obtained only in the laboratory.

In nuclear physics, considerable progress has been made toward obtaining the fission cross section of U^{233}--preliminary data are available up to 1000 ev. An excellent fit of the experimental eta and fission cross section data of U^{233} up to 4 ev has been obtained using the Wigner-Eisenbud multilevel formalism. A preliminary choice has been made to use two Fermi-type choppers separated in distance along the beam path and operating at a fixed phase difference for the study of the interaction of slow neutrons with moderating materials. The decay scheme for 11 hour Y^{93} is reported. The absorption cross section of Tm^{170} for pile neutrons has been found to be 150 barns. This value indicates that the flux destruction of Tm^{170} will not be a serious problem in the preparation of high activity thulium sources for radiography.

II. MTR PLANT ASSISTANCE

A. Technical Support to the Operation of the MTR

In addition to the routine service work undertaken at the request of Operations to maintain surveillance of the performance of the plant, the following items merited special attention during the third quarter.

1. Hydraulic Testing of Fuel Assemblies (W. C. Francis, J. R. McGeachin)

a. Single Assembly Test Loop

Early in this report period, the modifications were completed which were necessary to establish inlet flow conditions comparable to those in the MTR. These changes, amplified in the previous Quarterly Report, IDO-16297, comprised a modification of the inlet design of the fuel assembly holder, increased pump capacity to give a higher flow rate, and better temperature control of the water.

In order to establish, without doubt, that the static pressure detectors gave the same reading regardless of their location in the fuel channel, a test was performed in which static pressure tubes were inserted in different locations in a simulated fuel element channel. Pressure tops, drilled though one of the plates forming the channel, were used concurrently. Two static pressure tubes were used: one having holes parallel to the channel and, the other, perpendicular to the channel. Eight through-plate pressure holes were drilled at various locations so that readings could be taken from the center to the ends of the channel at the side plates. The static pressures determined at each of the sensing locations varied about as much as the pressure fluctuation in the water source, 0.1 psi. Considering the overall tolerances, this test indicates that the static pressure within the channel is uniform and that several different locations of tops or tubes may be used for measuring the average static pressure in the channel.

2. MTR Fuel Element Failure

One test on an ORNL-built MTR (nineteen-plate) fuel assembly produced very unexpected results. After this element was tested with a flow 10 percent higher than normal for reaction conditions, a bulge was noticed about three-fifths of the way down from the top of the fifth plate in from the concave side. The plate was distorted toward the convex side, the normal .117-inch channel measuring between 0.020 inch and 0.040 inch at the center of the bulge. The plate was cut out from the element for closer examination. It was found that, where the bulge occurred, the plate was not brazed to the side plates. The non-brazed section measured 11 inches in length on both sides. There was no noticeable change in thickness in the fuel plate where the failure occurred.

Should this type of failure occur during full power operation, rupture of the cladding might result because of the development of a hot spot at the bulge. No similar flaw has previously been observed in MTR fuel assemblies. It is most fortunate that this particular element was chosen for hydraulic tests. Although this fuel assembly was not inspected until it had received a 10 percent greater pressure than encountered in

the MTR, it may have deformed at even lower pressures. Inasmuch as the pressure required for deformation depends inversely upon the extent of the unbrazed length along the side plates, for a longer unbrazed length, the permissible flow rate would be lower. One point concerning operational safety should be mentioned; namely that, since boiling would occur before burnout, there is an excellent chance that the consequent instability in the neutron level would be noticed and the power reduced to below boiling conditions. Thus, because of operational procedures, a fuel plate rupture due to this cause is unlikely although possible.

a. Alpha Activity in the Process Water (E. H. Turk)

The alpha activity of the MTR process water has always run at a low, but detectable, level--well below tolerance limits. Other activity dominates the picture and determines the disposition of the water. However, the explanation of the occurence of the alpha activity has been unsatisfactory. Up to now, the source has been conjectured to be U^{235} which has been picked up inadvertently on the outside of the cladding during fabrication. New findings of this quarter suggest that it comes primarily from the U^{238} contamination in the beryllium reflector.

The lead, implying that contamination in beryllium might be the source, comes from the Pratt and Whitney plant at Livermore, California. In the course of their work in cutting a highly irradiated beryllium section of an MTR shim rod into sections, alpha activity was noticed and traced to Cm^{244}. From the neutron flux and the effective cross sections along the transuranic production chain, it was estimated that a contamination of about 100 ppm of U^{238} was sufficient to give the measured alpha activity.

To check this estimated value for U^{238}, an assay for uranium was carried out on the beryllium metal used to build the shim rod and the MTR reflector. As a matter of interest, the complete analysis was obtained using delayed neutron activation techniques. After neutron irradiation, this sample of beryllium metal was observed to produce delayed fission neutrons indicating the presence of a fissionable material, presumably natural uranium. The delayed fission neutrons were compared with those from the two U^{235} standards: 5.0×10^{-5} mg U^{235} and 1.0×10^{-4} mg U^{235}. The sample was calculated to contain 7.2×10^{-5} mg U^{235}. From the value of 0.7 percent U^{235} in natural uranium, the total uranium in the sample is 1.03×10^{-2} mg. This represents a concentration of 170 ppm natural uranium in the beryllium metal which was used to construct the MTR reflector. This value is in good agreement with the one from the calculations based on the observed Cm^{244} alpha activity.

The alpha activity in the process water and in the resin bed had been determined to be predominantly transuranic. Ninety percent is due to Cm^{244}, with minor contributions from Cm^{242}, Am and Pu. It thus seems likely that U^{238} is the major source of these alpha active isotopes and that the beryllium reflector is the primary source of U^{238}.

B. Auxiliary Facilities

1. Reactivity Measurement Facility (E. Fast)

The more important instrumental modifications which have been made to the RMF this Quarter are the following:

a) An expanded scale has been made for the regulating rod recorder to improve the accuracy to which the data chart can be read.

b) An electronic sequence controller was designed and built for automatically timing, to one millisecond, the time for registering a preset number of counts on a 4096 scaler. A new count is initiated at either 10 or 100 second intervals for accurate measurement of reactor periods. The mechanical features of the oscillator were completed and checked out satisfactorily.

a. RMF Oscillator (E. E. Burdick, G. L. Smith)

To provide a means for measuring absorption cross sections, resonance integrals, and other small-sample integral properties, an oscillator has been designed to be operated in the central water column of the RMF. In contrast with ordinary oscillator practice, the RMF system is relatively simple. Instead of maintaining fixed control rod positions and permitting the pile power to fluctuate in accordance with the k change associated with motion of the sample, the RMF kept in servo control during the entire cycle, the balancing regulating rod motion required is synchronously demodulated at the end points of motion (sample in or out), and the integrating circuit accepts no contribution while the sample is moving. The use of a calibrated control rod and a fairly simple demodulator gives a direct display of the k change associated with the absorption of the sample to a high degree of approximation.

b. Applications (E. Fast)

The more important applications of the RMF during this report period have been the following:

a) Thorium - RD-1 slugs were remeasured in the new stabilized lattice and found to give improved values of reactivity as a function of the delayed neutron assay for relative U^{233} content. Another group of 54 irradiated and two unirradiated thorium slugs were measured in the RMF. Reproducibility tests on a single sample gave a standard deviation of 3.1×10^{-6} $\Delta k/k$ or 0.39 percent of the quantity being measured.

b) WAPD-21 - A recheck was made of previous measurements on fuel rabbits, and calibration measurements on a series of new standards were carried out. Reproducibility is greatly improved over that observed with the previous lattice loading.

c) WAPD-28 - Preliminary calibration measurements were made on fuel samples.

d) Slugs containing burnable poisons in stainless steel were measured before and after irradiation in the MTR to determine poison burnout. The program is continuing to determine the useful life of such materials as a control rod constituent.

e) KAPL-37 - A somewhat detailed series of flux depression measurements were made on a mockup section of a loop experiment to be inserted in the MTR.

2. Machine Computation Facility (M. W. Holm)

General: The volume of work put out by the IBM 650 Computer has increased steadily throughout this Quarter and machine standby time has now become a negligible quantity. One part-time and three full-time programers handled the coding of new problems and the preparation of input data for "production runs", in addition to operating the computer. Reactor calculations continued to constitute a major fraction of the work, but routine processing of experimental and process-control data is becoming an increasingly important factor in machine utilization.

Noteworthy programs written during this period include a routine for performing a multi-level Wigner-Eisenbud fit to crystal spectrometer data, routines for calculating the worth of control rods, a routine which takes the output of PROD (reactor critical-radius and flux calculations) as input data and punches out radii and corresponding values of fast and slow fluxes in a form suitable for plotting, and routines for evaluating determinants, for performing "eta" calculations and for making least-squares fits. In addition, listing of 22 subroutines were received from IBM and two reactor codes were received from Westinghouse (APED).

Machine Utilization: In the box below are summarized the operating statistics for the three months making up this Quarter.

Month	Warm-up and Test-Deck Time	Scheduled Maintenance	Unscheduled Maintenance	Production Time	Standby time
July	6.38%	5.00%	11.43%	66.10%	11.09%
August	7.13%	5.83%	7.35%	77.13%	2.56%
September	5.09%	0.95%	0.30%	93.66%	0.00%

Production Time: Of the 428.6 hours of production time this Quarter, 20 percent were spent in checking out programs and subroutines, 80 percent in data reduction and problem solving. A further brief breakdown of the 80 percent data-reduction and problem-solving time follows:

Reactor calculations	67.77%
Data reduction (Cross Sections)	13.55%
Data reduction (SPERT-I)	9.12%
Data reduction (ICPP)	2.63%
Miscellaneous calculations	6.93%

Discussion: The application of the multilevel fit to cross section data is presented in the discussion of the Cross Sections' work effort. The applications of the reactor routines are further discussed in the section on Reactor Physics.

Analog Computer Development (R. S. Marsden): In order to utilize manpower economically, a conversion is being made of several analog computing projects to digital programs on the IBM-650. As long as computing time is available, the instrumentation required for the development of specific analog computers can be deferred. With this objective, several IBM programs have been developed to handle the problems which would have been solved by analog computers. For example, this Quarter, improvements were made in the IBM-650 computer program for multiplying polynomials to facilitate the machine's use in making numerical convolutions. Previously six instructions in the program had to be changed each time the sizes of the polynomials were changed. Now the sizes are entered as part of the data and the program automatically proceeds through a series of multiplications of varying size. The maximum size was increased from a multiplication of a 200-term polynomial by a 700-term polynomial to one of 400 terms by 1300 terms. The format of the input and output data was changed to permit use of a standard control panel.

3. Counting Room (C. H. Hogg)

In the course of supplying customary technical assistance to the operation of the plant and to the experimenters, the thermal neutron fluxes in two of the pneumatic facilities, VG-7 and VG-30, were measured over the vertical distance from the center line of the reactor to 11 feet above (Figures 1 and 2). These data are included in this report since they may be of interest to the designers of reactors. VG-7 is in the pebble zone, and VG-30 is at the interface between the pebble zone and the solid graphite region. Gold monitors were used in the flux measurements. The inflection in the curves at about 6 feet above center line concides with the 1-foot thick air gap above the graphite pebbles in the reactor. The leveling of the flux at some point, as it does at about 9 feet in both facilities, is to be expected because the neutron flux in the concrete approaches zero and streaming becomes the predominant contribution to the flux in the hole. It is somewhat surprising that both plots should level off at the same neutron flux. Since the bottom of VG-7 is about 2 feet below centerline and VG-30 is about 4 inches below centerline, the equivalence of the two limiting fluxes cannot be explained by assuming that the streaming flux originates at the bottom. The effective source of streaming must be considerably closer to the top end of the hole.

Apparatus Improvements: Seven new amplifiers and scalers have been received and are being installed in new relay rack enclosures with cooling fans. Ultimately all of the original electronics in the counting room, except the high pressure ion chamber, will be replaced with new equipment. The wire scanner has been improved with the addition of an isolation transformer and positive grounding of the chassis. A new interval timer and controller has been developed for use on the proportional counters. Units for all assemblies will be constructed as soon as time becomes available. Mechanism for an α scintillation detector has been

FIG. 1

THERMAL NEUTRON FLUX IN VG-30 AT A REACTOR POWER OF 40 MW

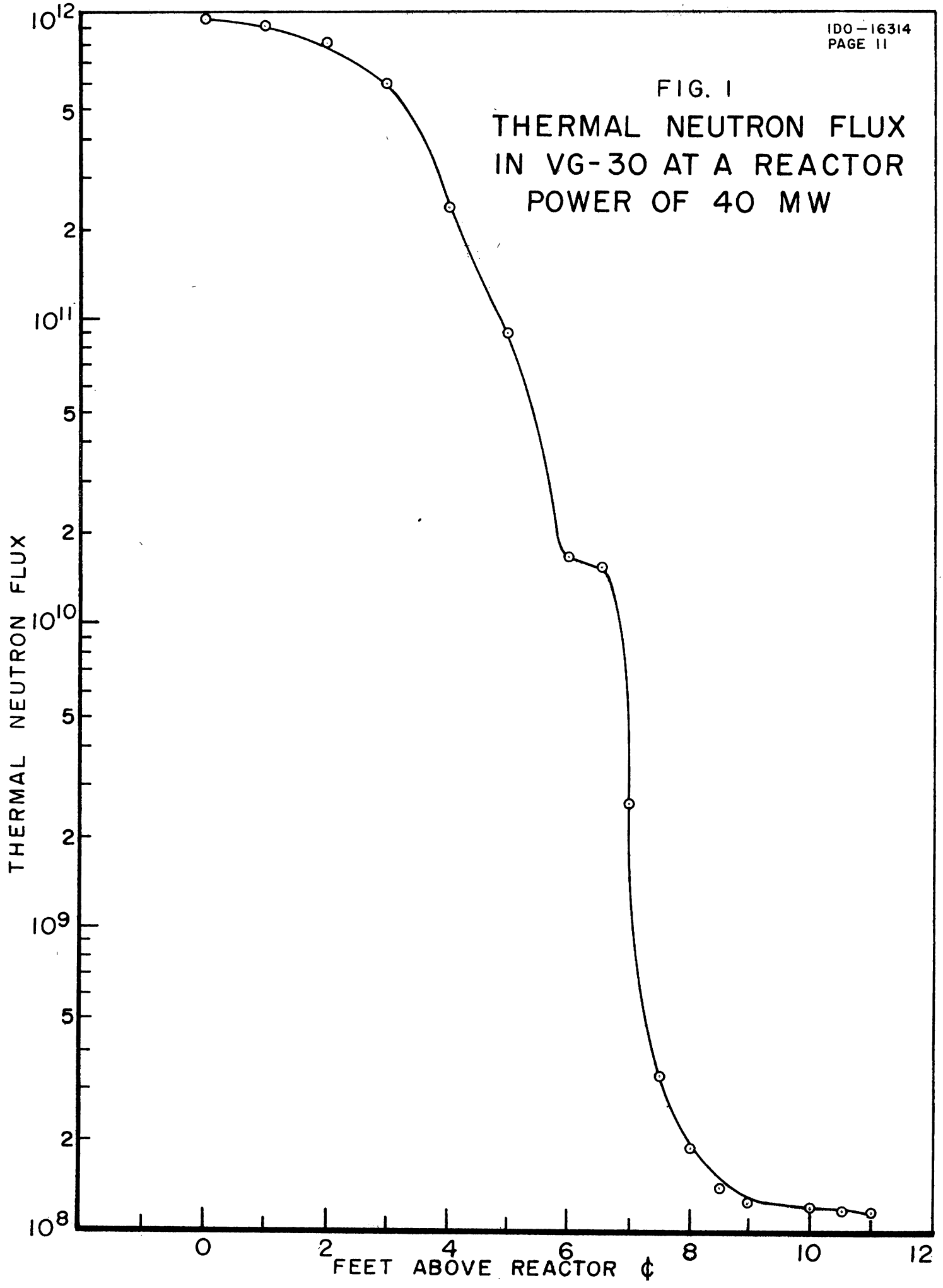

FIG. 2

THERMAL NEUTRON FLUX IN VG-7 AT A REACTOR POWER OF 40MW

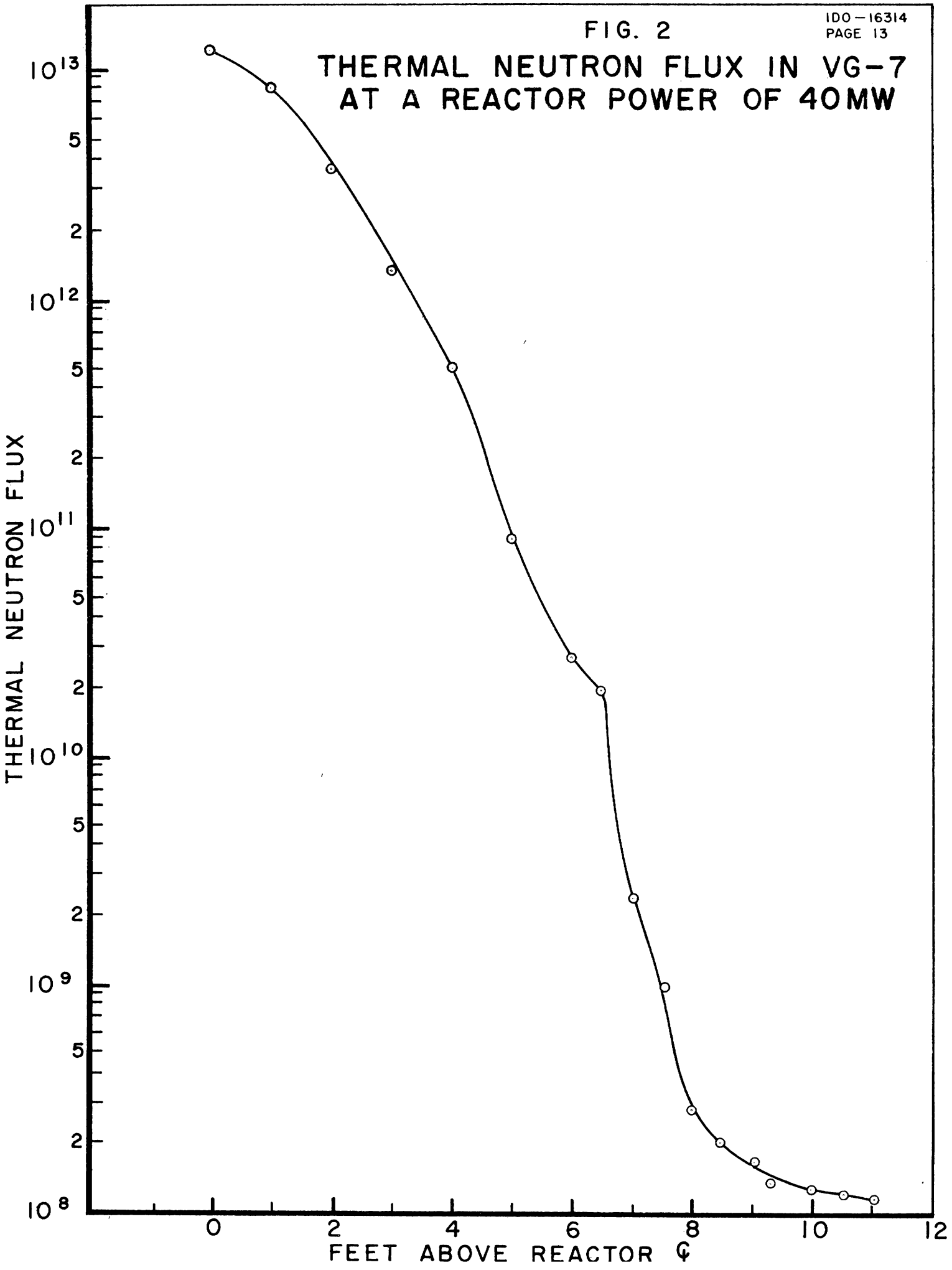

built and will be put into service when the electronics for it arrive. This unit will supplement the present NMC α proportional counter.

III. MTR-ETR DEVELOPMENT

A. Radiation Enhanced Corrosion of ETR Fuel Elements (W. C. Francis)

It is currently planned to incorporate the burnable boron poison of the ETR fuel elements in the aluminum cladding because of the difficulties encountered in alloying the boron with the fuel core. There is adequate evidence that boron alloys may be severely damaged after long exposure to a neutron flux. In the reaction B^{10} (n, α) Li^{7}, two heavy particles are produced which have considerable kinetic energy. Thus, embrittlement similar to that accompanying fission occurs. In addition, the volume of the products is about ten times that of the original B so that severe local stresses develop. The migration of the helium so formed to flaws in the alloy exaggerates the local stresses and causes internal cracking which further lowers the impact strength and provides a channel for corrosion pitting. Fortunately in ductile materials such as aluminum, the internal stresses can be relieved so that crack propogation is reduced and the damage is less critical. At the same time, boron, even in small quantities, greatly reduces the ductility of unalloyed aluminum. Thus from the literature information, and from previous laboratory corrosion tests run on B-Al alloys, it can only be concluded that damage through a radiation enhanced corrosion is possible and that further testing of the ETR alloy is necessary.

Previously scouting radiation-corrosion tests were made at the temperature of the MTR process water (115°F). Also autoclave tests have been carried out on unirradiated specimens at 300°F. These tests indicate that the corrosion resistance of the alloy is inferior to that of 2S aluminum. No tests have yet been made under the conditions of temperature and neutron flux equivalent to that in the ETR. Inasmuch as no in-pile loop facility is available for these corrosion tests, a compromise test is now in progress. Specimens of the ETR alloy have been irradiated in the A-40 position for one reactor cycle. These test samples are now in an autoclave at 277°F (the calculated maximum surface temperature of the ETR fuel elements). The change in weight will be followed for at least one cycle, then the temperature will be elevated in order to accelerate the test. 2S aluminum metal is being carried along as the control material.

B. Radiation Damage Studies (M. S. Robinson)

In order to be in a reasonably informed position for making safeguard evaluations of the ETR experimental facilities, the special alloys now proposed for these facilities will be tested for changes in physical properties after irradiation in a high neutron flux. The following alloys are being examined in the first series of tests: Zircaloy-2, Hastelloy-X, 2-1/4 Croloy, 410 Stainless Steel, Inconel-X, Inconel-702, and K Monel.

Arrangements were made with interested experimenters and fabricators to procure enough of these alloys for sufficient tensile and impact specimens to determine the effect of several irradiation conditions. Sixty percent of the materials have now been received with delivery of the last alloy scheduled for November 15, 1956.

Tensile and impact specimens are being fabricated at the Pocatello Naval Ordnance Depot Shop, with the exception of Zircalloy-2 samples which are being supplied by WAPD. GE-ANP will also supply some Inconel samples. Initial insertion of samples in the reactor is scheduled for November 12. Radiation periods are tentatively selected to be 2, 4, 8 and 12 or 16 cycles with both fast and slow flux monitoring provided during the course of the irradiation.

Tensile specimens will be accurately weighed before irradiation and will be tested in the MTR hot cell following irradiation. Hot cell tests will include descaling, weighing, hardness determination, tensile testing to destruction, and general observation of the specimens including photographs, if necessary. The broken specimens will be saved for future metallographic examination. Irradiation and cold control impact specimens will be sent to ORNL for testing and evaluation.

C. Fuel Element Development (W. C. Francis)

1. Sample Fuel Plates

A feasibility report covering perliminary fabrication studies of sample fuel plates was issued by the Sylvania Electric Company and has been approved by the New York Operations Office (October 19, 1956). The fabricated sample plates will not be available for several months.

2. Full Scale Assembly Development

Fabrication techniques for three types of fuel assemblies are sufficiently advanced in commercial plants to justify the procurement of full scale fuel assemblies without the small test-plate pilot evaluation. A fabricator has now been selected for supplying assemblies with powdered metal cores. Several possible fabricators are being considered for assemblies prepared from high strength aluminum and for assemblies having tubular geometry.

D. Film Boiling Experiment (A. W. Brown)

The film boiling experiment was proposed to obtain heat transfer data which would be directly applicable to the MTR. The heat transfer coefficient at the heat flux corresponding to the normal power level of 40 Mw is necessary in order to calculate the surface temperature of the fuel plates. It is also of interest to determine the heat transfer coefficients at higher heat fluxes up to the burnout point in order to guide future increases in the power of the MTR. In the proposal, data, therefore, are to be taken in the non-boiling, transition to boiling, and nucleate boiling regions. To be appropriate to the MTR, it is necessary to have this information for aluminum fuel plates. However, in order to avoid the hazard which might accompany melting of the aluminum fuel plates if the burnout heat flux were reached, an initial exploratory experiment was carried out with nichrome fuel plates so designed as to preclude melting of the plates at the burnout point. With this information as background, it would be possible to limit the heat flux when the aluminum plates are used to values well below the burnout conditions.

Two test sections designed for the burnout studies have been run. These test sections were selected to have different lengths, 3-inch and 6-inch, in order to measure any effect dependent upon the ratio of plate length to width. Each test section was composed of Nichrome fuel plates enclosing a water channel. The space at the back of each plate was packed with diatomaceous earth so that the heat flow would be only into the water channel. Iron-constantan thermocouples were mounted so as to measure both the inlet and exit water temperatures and thus obtain a heat balance giving the total heat flux in the test plates. In the tests, the inlet thermocouple did not function and the outlet thermocouple gave erratic readings. Thus the heat flux had to be calculated from the neutron flux and the fuel content of the plates. In each test section, the channel wall temperature was measured by a set of thermocouples on one fuel plate and the back wall temperature was measured by a set of thermocouples on the back of the other fuel plate. Space limitations made it unreasonable to attempt to put both sets of thermocouples on one plate. The channel thermocouples were made by inserting a 5-mil nickel wire through a hole drilled in one of the fuel plates. Saureisen cement was then packed around the wire in the hole and the end of the wire, on the channel side, was spot-welded to the bottom of a 7-mil deep groove cut into the Nichrome cladding. The groove and the nickel wire were then covered over with copper dental cement. The Nichrome lead wire of the thermocouple was then spot-welded to the back of the plate. The back wall thermocouples consisted of 10-mil chromel-alumel thermocouple wires which were spot welded to the back of the fuel plate at positions corresponding to the channel wall thermocouples (but on the opposite fuel plate). An aluminum-cobalt flux wire was present in each test section. From the integrated flux obtained from these wires, the reactor power (integrated over the time the test sections were in the reactor) and the fuel concentration in the plates, a value of the heat flux was calculated.

In the experiments, the two surface temperatures of the fuel plates, water channel side and insulated side, were measured at various reactor powers up to a calculated heat flux well beyond the predicted burnout point. At the higher heat fluxes, the thermocouple in the outlet water stream was sufficiently stable to indicate that the saturation temperature was reached even though it was too erratic to define the temperatures at lower heat fluxes.

A straight forward analysis of the data was made assuming that the measured temperatures and the calculated value of the heat input were correct, and that literature for both the fuel and core and that of diatomaceous earth was also proper. Two major unexpected results were derived from this straight forward approach: 1) The heat flux into the diatomaceous earth was very much greater than expected and was comparable in magnitude to that escaping to water; 2) The surface temperature of the metal on the water channel side was very much higher than the water temperature--20° to 500°F--which fact suggests an exceedingly high film resistance. The sharp rise in plate temperatures expected at burnout point did not occur. This rise may have been masked by the large heat loss toward the insulated side of the plate. However, a fairly abrupt change in the heat flux into the water channel occurred at a temperature between 700 - 800°F for both tests. Such a high temperature for the burnout point is very much higher than the 450°F which was expected from literature data on aluminum.

Because of these unexpected results, the important physical properties which had been taken from the literature--thermal conductivities of cladding, core and insulating material--are being remeasured. Also various other models are being explored in which a different set of independent variables are considered. For example, in the initial straight forward approach, the heat flux into the water channel was calculated from five variables, the two surface temperatures, the heat input, and assumed values for the thermal conductivity of the core and cladding. In another model, it was assumed that the temperature of the metal surface adjacent to the water was incorrect and therefore this variable was replaced by the literature value for the thermal conductivity of diatomaceous earth--equivalent to essentially zero heat losses through the back of the plate. The resulting calculations unfortunately predicted channel wall temperatures which were below the temperature of the reactor inlet water. Thus, this model is unsatisfactory. As a modification of this model, it may be assumed that there is a significant heat flow through the insulation because of water leakage into the insulated compartment. If one assumes a correspondingly higher thermal conductivity, the calculated water channel plate temperature rises up into the reasonable range. Experiments are under way to find out whether such thermal conductivities can be achieved by wetting the diatomaceous earth. Unfortunately with this approach, no quantitative value of the heat transfer coefficient can be obtained, but the results may be of value in explaining the experiment.

IV. REACTOR PHYSICS

A. ETR Critical Facility (W. J. Byron)

Many of the proposed experiments in the ETR will contain large quantities of fuel which will significantly affect the reactivity of the reactor. Also the experiments will significantly affect the flux distribution because of their large volume and large macroscopic effective fission and absorption cross sections. It will therefore be necessary to establish the reactivity values and flux distortions for all of the major experiments. In order to obtain these values without consuming valuable reactor time, an ETR Critical Facility will be built which will duplicate the nuclear properties of the ETR. With this reaction, it will also be possible to mock-up credible experimental mishaps so that the associated reactivity change can be determined. With this information, a more accurate safeguards evaluation of the experiment can be obtained.

The conceptual design of the ETR Critical Facility has been completed. The building design is also finished. It is expected ground will be broken October 17, 1956.

Core Design: The core is a duplicate of the ETR core except that the primary reflector will be 3 inches Be and 1-1/2 inches BeO in place of 4-1/2 inches Be. This change still gives a good fit to the calculated ETR core flux distribution. Mechanical designs of the lower support grid, shim rods and drives, and the support in the canal proper are complete. The design of the magnets themselves has not yet been selected. However, a type is under investigation now which shows promise. The main problem is due to the fact that the entire magnet assembly cannot be larger than 2-7/8 inch in diameter, although the magnet must lift 90 pounds with 75 Ma current and release in less than 10 milliseconds.

Control System: The relay wiring diagram is about 25 percent complete. The block diagram for the safety system is complete and the amplifiers and other instruments including recorders have been selected but not ordered. Standard components will be used to a great extent in order to save time and money. The servo system will be a larger (more powerful) version of the RMF system. Two spare CIC chambers have been released by SPERT and will be used in the critical facility.

B. Shielding Experiments Reactor Proposal (W. J. Byron)

Several organizations have expressed a need for a special irradiation facility in which to evaluate the performance of shield configurations and large instrumentation components in an environment of fast neutrons, thermal neutrons and gamma radiation. The preliminary design work of a suitable Shielding Experiments Reactor has been undertaken at the request of the Commission and is reported in PTR-124, "Shielding Reactor Proposal".

1. Conceptual Design

Early in the design work, it became obvious that a large core would be advantageous in order to provide a uniform flux over a wide cross sectional area. A parallelepiped with a central vertical hole was therefore selected as the geometry of the core (Figure 3). Design experience was available with this shape since it is similar to that of the RMF. Around this fuel box is placed a lead shield about 6 inches thick to attenuate the gamma radiation with as little weight of heavy shielding as possible. A 2-inch water-filled channel separates the fuel core from the lead shield to provide a cooling channel and to minimize positive reactivity changes should the lead shield be moved. The lead absorbs only about 3 percent of the thermal neutrons entering it and therefore does not appreciably depress the thermal neutron flux passing into the graphite thermal column.

Two types of experimental facilities are provided, one a "dry" volume for fast neutron irradiation, and a water-filled volume for shielding type experiments. Converter plates will be used in both types of facilities to obtain the desired fluxes. Neutrons are passed to the converter plate facing the dry volume along a graphite column flared outward from the reactor to encompass a 3 by 3 square foot cross sectional area of the converter plate. It is in this facility that the highest neutron flux is required--10-inch neutrons/cm^2/sec (>100 kev). A flux of 10^9 neutrons/cm^2/sec is adequate for the water-filled facilities.

The design parameters are briefly summaried in Table I.

TABLE I

Design Data for Shielding Experiments Reactor

Type		Thermal, enriched
Moderator		Water
Coolant (Primary)		Water (1000 gpm)
Coolant (Secondary)		Raw Water (1000 gpm) or air
Heat Exchanger		Shell-and-tube or fin
Critical Mass		$\sim$ 5 kg
Power		100 kw
Flux:	φ_{th} - Core average	10^{13} n/cm^2/sec
	φ_{th} - Center hole	3×10^{13} n/cm^2/sec
	φ_{th} - Into converter plate	10^{11} n/cm^2/sec
	φ_{f} - From converter plate	$\sim 1 \times 10^{11}$ n/cm^2/sec >100 kev
Heat production in lead		<30 kw, forced water cooled
Heat production in converter plate		$\sim$15 kw, air cooled

The control system will be similar to that of the MTR using level safeties and period channels double-tracked with fast-scram and sigma-bus electronics. There will be four block shim rods located in the corners for coarse control and a regulating rod for automatic operation. The rod moving and supporting frame work can be removed to allow access to the core. It is anticipated that the reactor will have to be refueled only once or twice a year.

2. Core Design Calculations (C. W. Reich)

Nuclear calculations for a Shielding Experiments Reactor have been carried out in order to make reasonably certain that the desired fast neutron fluxes of the order of 10^{11} neutrons/cm^2/sec and 10^9 neutrons/cm^2/sec with a fission spectrum of energies can be supplied. Since it is believed that the lower flux requirement could be easily satisfied if the higher flux is attained, the calculations are based on the production of the higher flux.

Several arrangements of shielding and thermalizing material were examined. The most satisfactory arrangement consisted of the core, 6 inches of lead, 2 inches of water, and a layer of graphite. A conventional two-group diffusion theory procedure was used in all the calculations. From the resultant flux and flux gradient at the face of the graphite column, the thermal neutron current into the converter plate was calculated. This current was then maximized by keeping the distance from the center of the core to the converter plate fixed and by adjusting the thickness of the graphite column. It was found that increasing the graphite thickness beyond

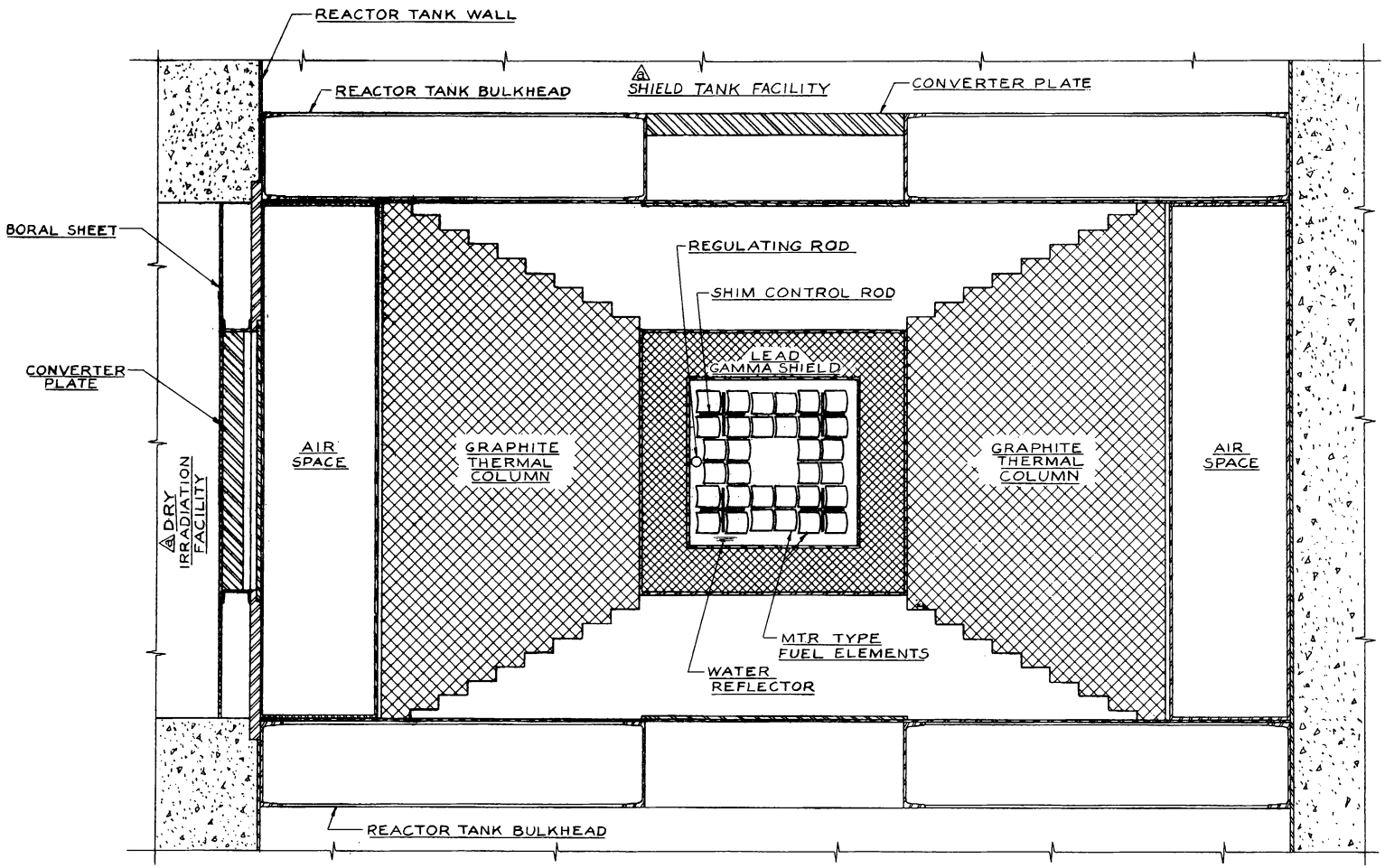

IDO – 16314
PAGE 21

FIGURE 3

APPROVED	PHILLIPS PETROLEUM COMPANY ATOMIC ENERGY DIVISION IDAHO FALLS, IDAHO
DATE	
W.T.S. 9-17-56	SHIELDING REACTOR PROPOSAL REACTOR PLAN PROPOSED ARRANGEMENT

REV. APP'D DATE	NO.	REVISION
	A	REPLACED THE WORD "SANDIA" WITH "DRY" ADDED SHIELD TANK FACILITY IN PLACE OF IRRADIATION FACILITY. 9-17-56

SCALE 1/8" = 1'-0"		DATE	AFE NO.
DESIGNED			DRAWING NO. REV.
DRAWN	G.M.P.	9-18-56	MTR-D 450L a
CHECKED			SHEET NO. OF
APPROVED			

about one diffusion length (50 cm) markedly decreased the neutron current into the plate. The fast flux out of the converter plate was calculated in terms of the thermal flux incident upon it, assuming isotropic production of fission neutrons and negligible capture of the fission neutrons in the plate. The following table summarizes the results of the calculations for the two types of converter plate considered: 1) 3-inch thickness of natural uranium (9 sq. ft. area), and 2) 50-mil thickness of highly enriched U^{235} (with an area of 9 sq. ft.).

TABLE II

Type of Plate	Graphite Thickness	ϕ_f From Plate* / ϕ_{th} Into Plate	ϕ_f From Plate* / ϕ_{th} Core Avg.	Avg. ϕ_{th} in Core* to give 10^{11} n/cm^2 sec. From Plate
50 mil Enriched Uranium	47.67 cm	3.84	0.0122	0.82×10^{13} n/cm^2 sec
	78.15	3.84	0.00419	2.39×10^{13} n/cm^2 sec
3" Natural Uranium	47.67 cm	1.31	0.00415	2.4×10^{13} n/cm^2 sec
	78.15 cm	1.31	0.00143	7.0×10^{13} n/cm^2 sec

* The fast flux is measured at a distance of 1 cm along the axis normal to the plate through its center. The distance from the plate to the center of the core is fixed at 6 feet.

C. Evaluation of 20% Enriched Fuel for High Flux Reactor (H. L. McMurry, R. Haldin)

The Commission has asked for a demonstration of the fact that a high flux testing reactor (not significantly inferior to the MTR) can be designed using commercially fabricated 20% enriched fuel. It is therefore planned to procure a full core loading of 20% enriched fuel assemblies for the MTR in which the radiation stability and lifetime in MWD will be clearly indicated. As a starting point, specifications for the geometry of the fuel assemblies have been set which duplicate that now in use in the MTR. An attempt to develop a suitable fabrication procedure using wrough metallurgy techniques is in progress in one commercial laboratory and a parallel approach based upon powder metallurgy is being initiated in another laboratory. In the wrought system, difficulty has been encountered in rolling the aluminum alloy containing the high uranium content necessary for the core material. This problem can be ameliorated somewhat by increasing the fuel meat thickness.

As an accompanying study, estimates of the charge life of the MTR when fueled with uranium enriched to 20 percent in U^{235} relative to that obtainable using regular MTR (highly enriched) fuel were made, assuming the following conditions.

1) Twenty percent enriched fuel assemblies identical in U^{235} content and dimensions with present MTR design.

2) Twenty percent enriched fuel assemblies identical in U^{235} content but with plate thickness 0.060 inch instead of 0.050 inch. Consideration of this change was requested by a potential fabricator. It raises the metal/water volume ratio and thus reduces the charge life.

For case 1, the charge life of the 20 percent enriched fueled reactor relative to the MTR fueled reactor was based on the method described in MTRL-54-110. This procedure involves a perturbation theory approach which permits account to be taken of the burnout distribution of the fuel. For present purposes the working equation reduces to

$$\frac{T_{20\%}}{T_{MTR}} = \frac{[\Sigma^o - \delta\Sigma^o - y\,\Sigma^o_F]}{[\Sigma^o - y\,\Sigma^o_F]} \qquad (1)$$

where

$T_{20\%}$ = MWD charge life with 20 percent enriched fuel

T_{MTR} = MWD charge life with MTR fuel

Σ^o = Macroscopic cross section due to that uniformly distributed poison which makes the MTR just critical with fresh fuel present and no xenon present. This quantity was calculated using the theory in MTRL-54-110 and assuming that a full load of fresh 200 gram MTR assemblies would run 650 MWD. This assumption corresponds to present conditions.

Σ_F^o Macroscopic fission cross section with fresh fuel present.

y Total fission yields (direct + indirect) for Xe^{135} and Sm^{149}.

$\delta\Sigma^o$ Change in Σ^o due to a reduction in p from 1.0 (MTR value) to 0.93 (20 percent enriched value). This was calculated by perturbation theory using Equation (30) of IDO-16252.

The effect of increasing the metal/water volume ratio by increasing the thickness of the fuel plates from 0.050 inch to 0.060 inch was considered to be additive. This was calculated from the slope of the plot in Figure 4, which shows how the weighted critical mass in the MTR varied with metal/water volume ratio during part of 1953, when fuel assemblies with lower metal/water ratio were introduced into the core. While the present experimental load would undoubtedly cause this curve to be displaced upward, the slope is expected to be about the same. (Differences in weighted critical mass are numerically equal to MWD gain or loss). Using Figure 4 and the difference in metal/water ratio on going from 0.050 inch plates to 0.060 inch plates, the loss in charge life was estimated.

During operation of the reactor some plutonium is produced by resonance capture and thermal capture in U^{238}. Assuming all of this plutonium is available to compensate for lost U^{235}, about 10 percent more charge life is predicted. Table III summarizes the results of these calculations.

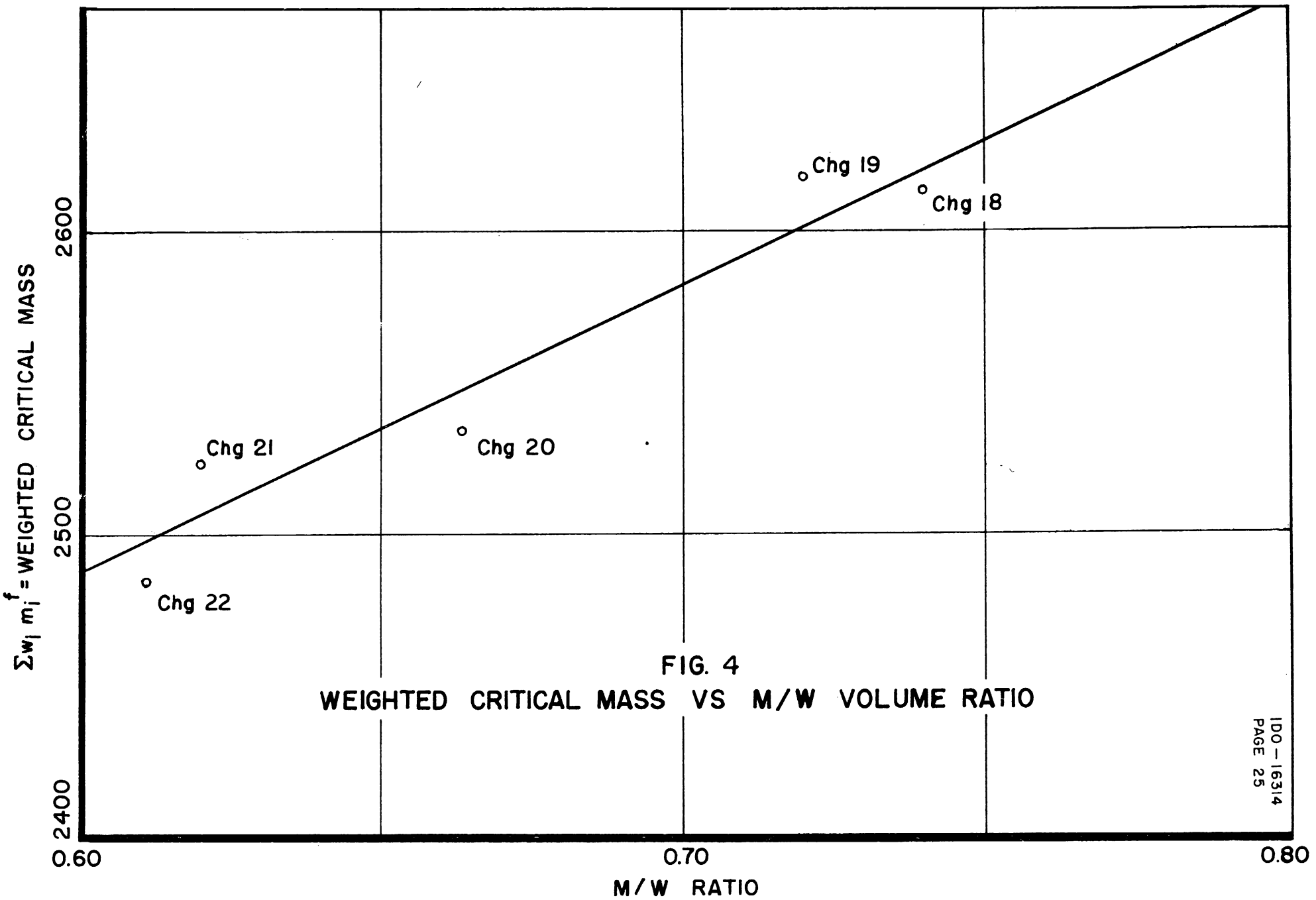

FIG. 4
WEIGHTED CRITICAL MASS VS M/W VOLUME RATIO

TABLE III

Charge Lives of MTR with Conventional Fuel and 20% Enriched Fuel

Core	Plate Thickness (inches)	Metal/H_2O Volume Ratio	MWD Predicted (w/o Pu^{239})	MWD Predicted (with Pu^{239})
MTR Fully Enriched	0.050(a)	0.72	650(b)	650
20% Enriched	0.050	0.72	400	415
20% Enriched	0.060	0.86	270	285

(a) MTR has two plates 0.060" and 17 plates 0.050".

(b) 650 MWD predicted for current operating conditions by method given in IDO-16140.

Additional data showing the ratio of charge life with 20 percent enriched fuel to charge life with MTR fuel as a function of U^{235} content were also obtained using Equations (1). The same fuel assembly design was assumed and no credit for Pu^{239} was taken. Figure 5 is a plot of these results.

D. Critical Size Calculations for SPERT III with Stainless Steel Fuel Assemblies (D. R. Metcalf)

Calculations on critical sizes were made for a proposed SPERT III reactor with stainless steel fuel assemblies using the three and two group constants given in the second Quarterly Report, IDO-16297. This was treated as a two region problem with a core metal to water volume ratio of .34. The entire core material was treated as homogeneously distributed. The following Table IV summarizes these results.

TABLE IV

Critical Size Estimates for Stainless Steel SPERT III Core

Temp.	Constants Used	(cm) Core Radius	Number of 638 gm F.A.	(kg) Critical Mass
68°F	Three Group Table I PTR-102	17.8	~ 16	10.2
650°F	Three Group Table I PTR-102	30.5	~ 46	29.3
68°F	Two Group Table II PTR-102	15	~ 11	7
650°F	Two Group Table II PTR-102	26.3	~ 35	22

The three group critical size estimates are consistently higher than the corresponding two group critical size. Further study is needed to account for this discrepancy.

The effect of a 1/8-inch ring of stainless steel around the reactor core was also estimated. The radius was increased 4.7 percent at 68°F and 6.2 percent at 650°F by this change.

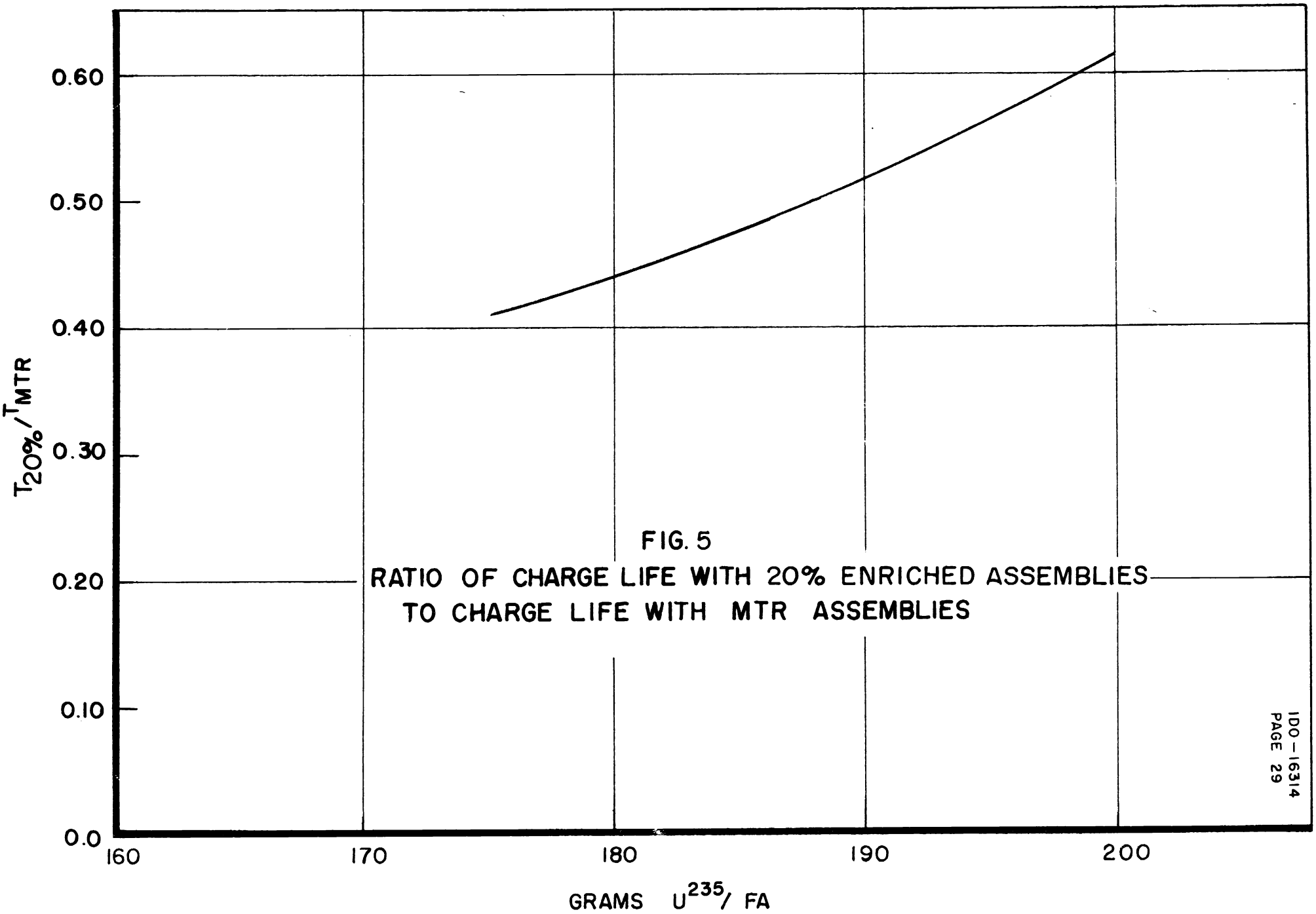

FIG. 5

RATIO OF CHARGE LIFE WITH 20% ENRICHED ASSEMBLIES TO CHARGE LIFE WITH MTR ASSEMBLIES

E. High-Flux Test Reactor

There appears to be a need for a reactor for materials tests in which the thermal and fast fluxes available are significantly higher than those obtainable in the MTR. This need has been discussed in PTR-81. Since the experience of Phillips AED concerns thermal reactors, this type is considered first. A scoping investigation has been initiated with the principal objective of learning what moderator, coolant, and reflector are most attractive for a high-flux test reactor. Another objective is to determine the maximum fluxes attainable by employing dilute fuel. One good reactor configuration is that employed by the Reactivity Measuring Facility. This design consists of an annulus of fuel surrounding a central hole in which those experiments requiring the highest flux will be located. The fuel, in turn, is surrounded by a reflector, probably of the same material which occupies the central hole. In this preliminary survey five sizes of holes were considered, 2.5 cm radius up to 40. This flux-trap principle was employed by a 1956 ORSORT Group for their design of a High Flux Research Reactor; they used D_2O as the moderator, coolant, and reflector.

Three situations have been considered briefly in the study of moderators, coolants, and reflectors. Each employs an annulus composed of 168-gram MTR fuel assemblies. In Case I the fuel is cooled and moderated with H_2O; light water occupies the central hole and also surrounds the fuel. In Case II, D_2O is the coolant, moderator, and reflector. Case III employs the same reactor core as Case I; however, beryllium (cooled with light water) occupies the central hole and surrounds the core. The experiments which will be located in this high-flux facility are simulated by a hollow stainless steel cylinder; the dimensions of the cylinder for each size of central hole are given in Table V.

Information concerning maximum fluxes attainable was obtained by studying a D_2O reactor with a 20 cm central hole. Four fuel element loadings were considered: 168, 100, 50, and 25 grams of U^{235} per assembly.

Based on a scoping investigation of very high flux testing reactors employing the RMF or flux-trap design and considering only the problem of heat dissipation, maximum thermal and fast neutron fluxes of 10^{15} and several by 10^{15} neutrons/(sq. cm, sec.), respectively, appear attainable in experiments which are gray absorbers. This conclusion is predicated on a maximum local heat flux of 2.5×10^6 Btu/(sq. ft., hr.). If a central experimental facility with a radius of less than about 10 cm is desired, H_2O testing reactors appear most attractive. When a larger central hole is needed, the choice would probably be a D_2O machine. The estimated operating power levels of these high flux testing reactors appear to be in the range of 100 to 500 megawatts.

Somewhat higher fluxes can be obtained using sodium as the core coolant and H_2O as the moderator in the central hole. Sodium has two advantages: it reduces the moderation in the core proper, thus supplying more fast flux to central hole; it provides a higher heat flux--a value 6×10^6 Btu/sq. ft./hr. being reported in laboratory work. Calculations are in progress to establish the quantitative magnitude of these advantages.

1. Nuclear Calculations

Two-group calculations based on diffusion theory were made for both the perturbed and unperturbed situations; the term perturbed, refers to the presence of the hollow stainless steel cylinder in the central hole. The nuclear constants employed are recorded in Table VI. In Cases I and III 19-plate fuel elements with aluminum/water ratio of 0.664 were used; concerning D_2O reactors, 18-plate assemblies with aluminum/water ratio of 0.7 were employed because of the availability of the nuclear constants. The assumed height of the reactor core and reflector savings was 78 cm, which is the MTR value, in all cases except when 50 gram and 25 gram fuel assemblies were employed; the values used in these other two situations were 110 and 156 cm, respectively. The thickness of fuel annulus required for criticality was established, and flux distributions were computed for each situation. Some of the principal results are presented in Tables VII and VIII. Calculated maximum neutron fluxes in the central hole, with and without experiments, for the three cases considered, are given in the top half of Table VII and in Figures 6 and 7. These values permit comparison of the flux levels which can be achieved with each system. Maximum fluxes in the 20 cm central holes of four D_2O reactors employing different fuel concentrations are presented in the top half of Table VIII. The cross-sectional areas and relative core volumes, respectively, of the fuel annuli for the just-critical reactors are given in the bottom half of each table. This information is an approximate index of the required operating power level of each reactor system.

The flux values presented in Table VII and VIII are based on a maximum local steady-state heat flux of 2.5×10^6 Btu/(sq. ft., hr.), which is the highest heat flux having been demonstrated to date in the laboratory. In the design of a high flux test reactor, considerations of heat dissipation could further limit the operating power and flux levels attained. On this basis the maximum fission rate with 19- and 18-plate MTR fuel assemblies are 0.94 and 0.89×10^{14} fissions/(cc, sec). The resulting maximum thermal fluxes in reactor cores with various fuel concentrations are given in Table IX. It is assumed that the limiting heat flux with H_2O can also be applied directly to D_2O.

Although the location of maximum fluxes are as expected, it is desirable to mention them. The maximum thermal flux in fuel is at either the inside or outside boundary, depending on the size of hole and contained experiment, if present. Maximum thermal and fast fluxes in the experiment are at boundary nearest fuel, except the thermal flux for hollow cylinder in 2.5 cm hole wherein maximum value is at the inside boundary. Concerning the central hole without the experiment, the maximum fast flux is at fuel boundary. Maximum thermal flux is at center, except for the larger holes with light water and with beryllium in which it occurs nearer the fuel.

2. Effect of Moderator, Coolant, and Reflector

For each of the three cases considered, the maximum unperturbed thermal flux passes through a maximum as the hole size increases, the highest thermal flux being obtained with a D_2O reactor and the lowest with beryllium. The maximum with Cases I, II, and III are 3.4, 4.2, and 2.4×10^{15} neutrons/(cm^2, sec) and are obtained when the radii of the central

hole are about 5, 20, and 20 cm, respectively. With light water maximum thermal flux is attained with a small hole because H_2O is a very good moderator; in addition, with only a small volume of light water its large capture cross section cannot assert itself. With D_2O and beryllium, maximum thermal fluxes are obtained at a radius of approximately 20 cm because essentially complete neutron moderation is effected in this distance. Since the capture cross section of heavy water is negligible and that of beryllium is quite small, the moderating property of each appears dominant.

The maximum unperturbed fast fluxes are equal to or greater than the corresponding maximum thermal fluxes. In Cases I and III the maximum fast fluxes pass through minima at a 20 cm radius with values of 3 and 4 x 10^{15}; with D_2O the minimum probably occurs at 40 cm and is 4 x 10^{15}. When the radius of the central hole is less than 30 cm, the highest fast fluxes are attained with D_2O reactors; with radii greater than 30 cm, the fast fluxes with Case III are highest. The curve for H_2O reactors is below those for the other two cases.

The perturbed results and this discussion apply to those situations in which the experiments are simulated by the stainless steel hollow cylinders of Table V. In all cases with a central-hole radius of about 15 cm the maximum thermal fluxes are in the range between 0.7 and 0.8 x 10^{15} neutrons/(cm^2, sec). The curve for D_2O reactors is quite flat, and maximum perturbed thermal fluxes of 0.8 x 10^{15} are attained with central-hole radii up to at least 40 cm. With H_2O reactors these maximum values increase markedly as the sizes of the central hole and experiment are reduced, a perturbed thermal flux of approximately 1.4 x 10^{15} being obtained with that situation in which the radius of the central hole is 5 cm. The thermal flux values for Case III are usually second-best.

With experiments present, the maximum fast fluxes decrease markedly as the size of the experimental facility is increased. For the situations considered highest fast fluxes are obtained with D_2O reactors and lowest with H_2O machines, because D_2O is a poorer moderator than H_2O. With a 20 cm central hole the maximum perturbed fast fluxes with D_2O and H_2O are approximately 4.5 and 1.5 x 10^{15}, respectively.

A tabulation of some neutron and heat fluxes for the Engineering Test Reactor and for one D_2O embodiment of a high flux test reactor is presented below. Although direct comparison of the results from these two reactor systems is not proper, the performance of the ETR does serve as a good reference. Two operating situations should be remembered when considering this tabulation: a) in the unperturbed case with the ETR the experimental facilities contain aluminum pieces, and aluminum is a strong neutron absorber compared to D_2O; b) the ETR experiments will probably contain significant amounts of fuel, whereas the non-fissionable neutron absorber, stainless, steel was employed to simulate experiments in this study.

Some Neutron and Heat Fluxes

		ETR	D_2O Reactor with 20-cm-radius Hole
		Maximum Neutron Fluxes x 10^{-15}, neutrons/(sq. cm., sec.)	
Without Experiments:	Thermal	0.84	4.2
	Total	2.8	8.6
With Experiments :	Thermal	0.63	0.77
	Total	3.3	5.2
		Maximum Heat Fluxes x 10^{-6}, Btu/(sq. ft., hr.)	
		1.15	2.5

3. Reactor Size and Power

The variation of the cross-sectional area of the fuel annulus with size of the central hole for the just-critical reactors is shown graphically in Figure 8. The critical sizes of the unperturbed D_2O reactors have a minimum at a radius of 20 cm. For all other situations considered the reactor size increases markedly with the size of the experimental facility and the experiments, if present; the reactor volume increases about four-fold as the radius of the central hole increases from 5 to 40 cm. The unperturbed and perturbed reactors of Case III are the smallest because water is an excellent neutron moderator and beryllium is an excellent neutron reflector.

An indication of the operating power of the actual testing reactors is obtained by considering the smallest reactors of Case III, which approximate the MTR. If the MTR could operate with a maximum heat flux of 2.5×10^6 Btu/(sq. ft., hr.), its operating power would be about 100 MW. It is estimated that a crude approximation of reactor power can be obtained by applying a factor of 1/5 to 1/10 to the cross-sectional areas presented in Table VII and Figure 8, i.e. about one megawatt of power would be generated in an actual testing reactor for every 5 to 10 cm^2 of cross-sectional area of the fuel annulus of the just-critical reactor. Therefore, the operating power levels of the high-flux test reactors being considered in this study would probably vary from about 100 to 500 megawatts. It is appreciated that the cost of the U^{235} fuel consumed by a high-power testing reactor and the cost of heat dissipation are sizeable expenses. However, since the value of the experiments is so much greater than these expenses, the neutron fluxes attained in the advanced testing reactor should be the over-riding consideration.

4. Effect of Fuel Concentration on Fluxes

In order to study the effect of fuel concentration on flux, four concentrations were considered in connection with D_2O testing reactors each

having a 20 cm radius experimental facility; the four concentrations are 168, 100, 50, and 25 grams of U^{235} per MTR fuel assembly. The principal results are summarized in Table VIII. The thermal and fast neutron fluxes for both the unperturbed and perturbed situations increase markedly as the fuel concentration is reduced. For example, the maximum thermal flux in the hollow stainless steel cylinder increases from 0.77 to 10^{15} with 168-gram fuel to 3.5×10^{15} neutrons/(cm^2, sec.) with 25-gram assemblies. In order to achieve this nearly five-fold increase in thermal neutron flux it is necessary to increase the reactor volume and operating power level approximately ten times; if the operating situation associated therewith is practical, this price appears reasonable for the results obtained.

TABLE V

Simulated Experiment in Central Hole
(Hollow Cylinder of Stainless Steel)

Radius of Experimental Hole, cm	Radii for Hollow Cylinder, cm	
	Inside	Outside
2.5	1.25	1.75
5	2.5	3.5
10	5	7
20	10	14
40	20	28

TABLE VI

Nuclear Constants

	Σ_a, cm^{-1}	Σ_f, cm^{-1}	D_s, cm	L^2, cm^2	D_f, cm	τ, cm^2
H_2O	0.0197	--	0.160	8.12	1.19	33
168-gram Fuel Elements Plus H_2O	0.0799	0.0540	0.259	3.24	1.31	61
D_2O	0.000080	--	0.830	10400.	1.28	126
168-gram Fuel Elements Plus D_2O	0.0696	0.0540	1.230	28.2	1.65	262
100-gram Fuel Elements Plus D_2O	0.0437	0.0321	1.230	28.2	1.65	262
50-gram Fuel Elements Plus D_2O	0.0246	0.0161	1.230	28.2	1.65	262
25-gram Fuel Elements Plus D_2O	0.01505	0.00803	1.230	28.2	1.65	262
Beryllium and 3 v/o H_2O	0.00178	--	0.825	464.	0.601	88
168-gram Fuel Elements Plus H_2O	0.0799	0.0540	0.259	3.24	1.31	61
Stainless Steel	0.2022	--	0.444	2.20	1.39	600

TABLE VII

(1) Calculated Maximum Neutron Fluxes

(Core is H_2O-cooled and -Moderated)

Radius of Experimental Hole, cm	CASE I: H_2O				CASE II: D_2O				CASE III: Be + 3 v/o H_2O			
	(2) Perturbed		(3) Unperturbed		Perturbed		Unperturbed		Perturbed		Unperturbed	
	Thermal	Fast	Thermal	Fast	Thermal	Fast	Thermal	Fast	Thermal	Fast	Thermal	Fast
2.5	1.71	5.4	2.64	4.1								
5	1.46	4.5	3.4	3.3					1.05	5.3	1.94	5.0
10	1.01	3.06	3.07	3.06	0.81	6.1	3.05	6.4	0.81	4.4	2.23	4.2
20	0.60	1.62	2.61	3.02	0.77	4.4	4.2	4.5	0.66	3.04	2.40	3.8
40	0.245	0.56	2.37	3.2	0.78	2.36	3.5	3.9	0.53	1.41	2.28	4.4

(4,5) Cross-Sectional Area of Fuel Annulus, cm^2 (Approximate Index of Reactor Power)

2.5	1110	1030						
5	1340	1200					510	400
10	1930	1840	2450	1170			760	480
20	3100	3140	3770	1030			1240	770
40	5490	5460	5390	1750			2030	1550

(1) Multiply all values by the factor, 10^{15}
(2) Values for perturbed case pertain to maximum values in hollow stainless steel cylinder which simulates some experiments.
(3) Values for unperturbed case pertain to maximum values in central hole without experiments.
(4) Height of reactor core plus reflector savings is 78 cm.
(5) A crude approximation of reactor power can be obtained by employing a factor of 1/5 to 1/10, i.e. about one megawatt of power would be generated in an actual testing reactor for every 5 to 10 cm^2 of cross-sectional area of fuel annulus of the just-critical reactor.

TABLE VIII

Maximum Neutron Fluxes in D_2O Test Reactor, x 10^{-15}
20 cm Central Hole

Grams U^{235} per Fuel Element	Perturbed		Unperturbed	
	Thermal	Fast	Thermal	Fast
168	0.77	4.4	4.2	4.5
100	1.20	5.9	6.7	7.0
50	2.50	9.7	10.8	8.4
25	3.5	10.5	19.6	12.6

	Relative Volume of Reactor Core	
168	3.6	1.00
100	7.6	2.89
50	9.5	3.4
25	39.	16.6

TABLE IX

Maximum Fission Rates and Thermal Fluxes in
Ractor Core

Grams U^{235} per Fuel Element	Σ_f, cm^{-1}	19-Plate Fuel Assembly		18-Plate Fuel Assembly	
		Fission Rate, Fissions cc, sec	Thermal Flux, Neutrons cm^2, sec	Fission Rate, Fissions cc, sec	Thermal Flux, Neutrons cm^2, sec
168	0.0540	0.937×10^{14}	1.736×10^{15}	0.894×10^{14}	1.655×10^{15}
100	.0321	0.937×10^{14}	2.920×10^{15}	0.894×10^{14}	2.784×10^{15}
50	.0161	0.937×10^{14}	5.84×10^{15}	0.894×10^{14}	5.57×10^{15}
25	.00803	0.937×10^{14}	11.68×10^{15}	0.894×10^{14}	11.14×10^{15}

Bases: Maximum heat flux = 2.5×10^6 Btu/ (sq. ft., hr.)
3.15×10^{10} fissions/sec = 1 watt
Surface to volume ratio is same as in MTR core. MTR volume is 1.0209×10^5 cc; surface areas of fuel meat are 3.853 and 3.673×10^5 cm^2 with 19- and 18-plate fuel assemblies.

FIG. 6

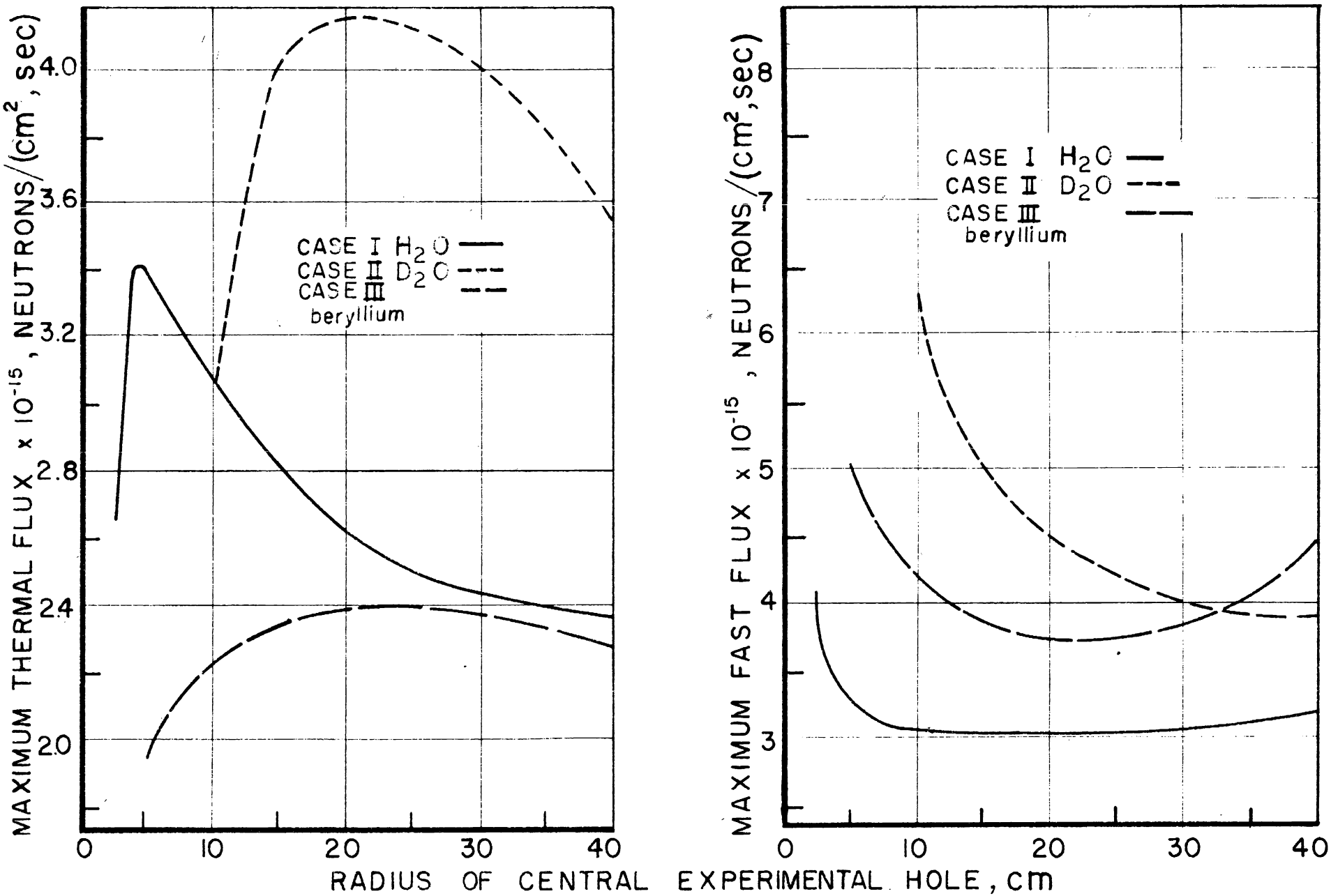

MAXIMUM NEUTRON FLUXES IN CENTRAL HOLE WITHOUT EXPERIMENTS

FIG. 7

MAXIMUM NEUTRON FLUXES IN SIMULATED EXPERIMENTS

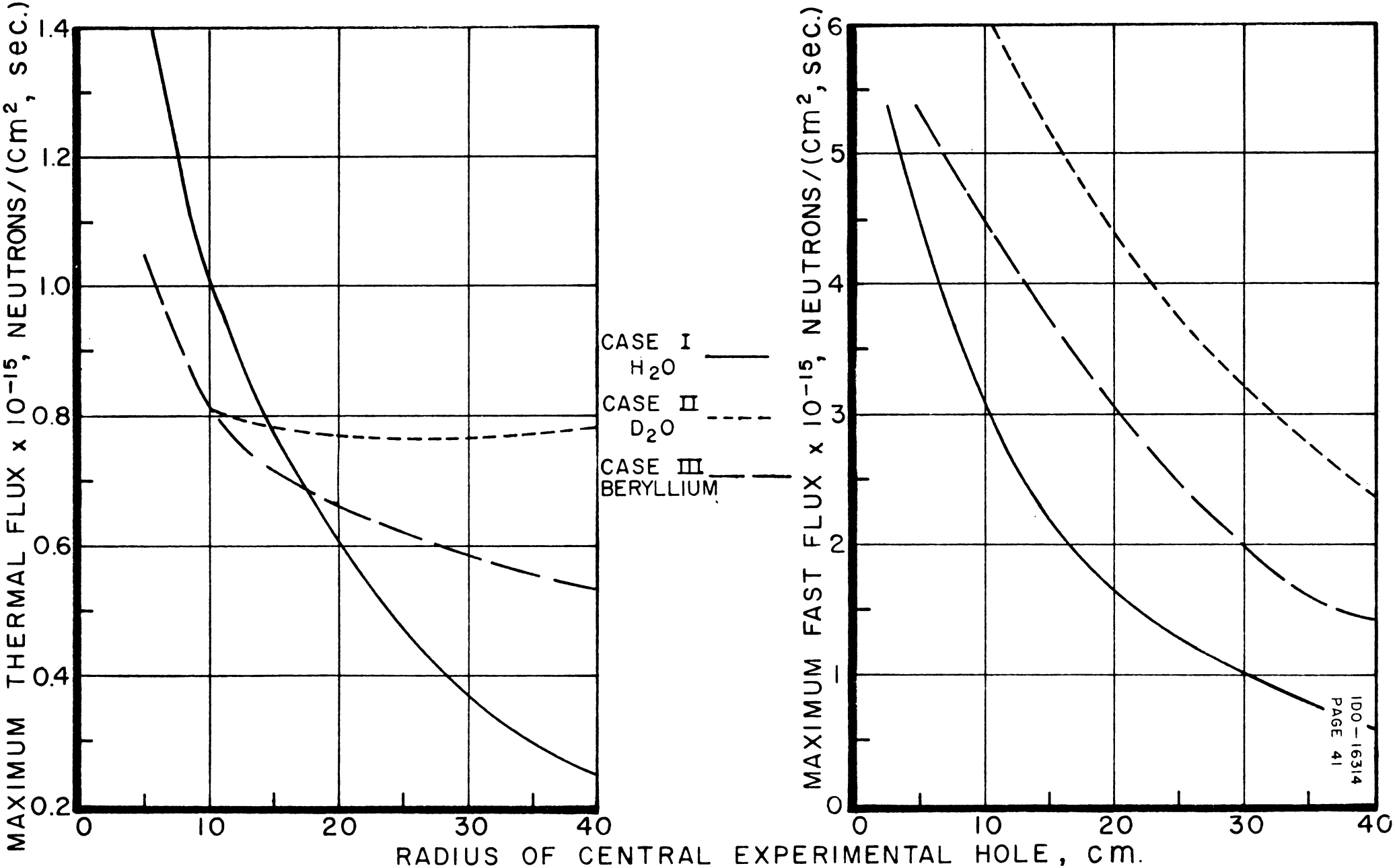

FIG. 8

APPROXIMATE RELATIVE REACTOR POWER LEVELS

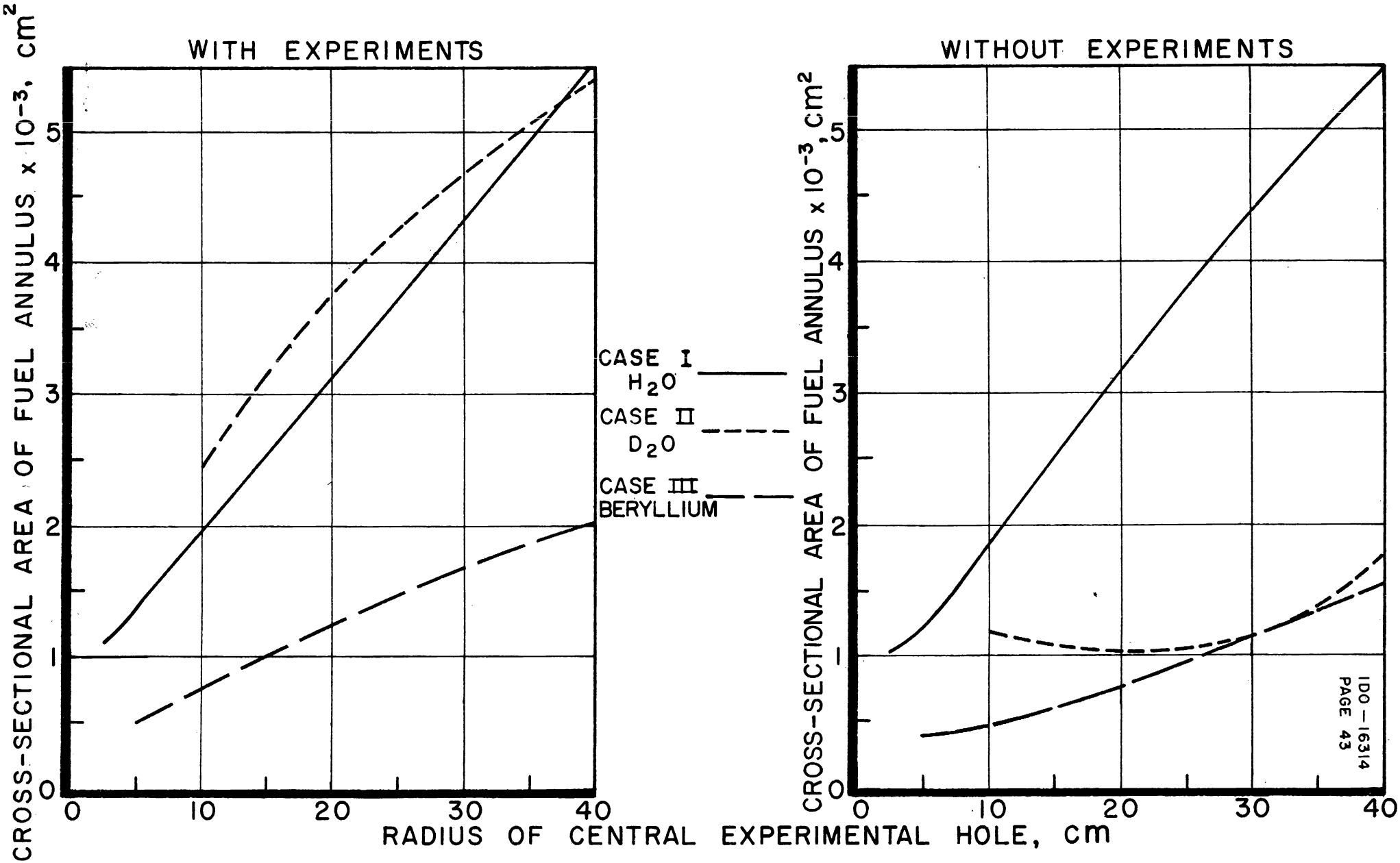

F. Thorium Program (E. Fast)

The objectives of the thorium program are to measure the changes in reactivity due to fuel and poison production in thorium as a function of integrated neutron flux, and to determine the influence of slug geometry on the effectiveness of these changes. Ultimately fundamental constants important to reactor design will be obtained.

RD-1 - Thorium slugs irradiated under the RD-1 program up to a total calculated exposure of 1.29×10^{21} nvt were measured again in the RMF after mechanical alterations had been made in this test reactor to stabilize the lattice. The results are plotted in Figure 9 showing the net reactivity (compared to an unirradiated slug) as a function both of the calculated grams of U^{233} and of the relative assay for U^{233} based upon the delayed neutron activity. These data indicate that the flux information used in calculating exposure is somewhat uncertain. The standard deviation in repeated measurements of reactivity gave 4.3×10^{-6} $\Delta k/k$ for an unirradiated and 2.3×10^{-6} $\Delta k/k$ for an irradiated slug. Flux depression, as measured with indium foils, was 0.5 at the surface. However, the net effect of U^{235} at the center of a slug on the reactivity of the RMF was shown to be only 17 percent less than at the surface.

Discussion - Prior to continued irradiation in the MTR it is necessary to determine the U^{233} gram content of the RD-1 slugs in order to insure that permissible slug temperatures will not be exceeded. Inasmuch as it has proved to be difficult to obtain chemical analysis for these slugs from outside laboratories, it is planned to derive the desired U^{233} content from delayed neutron data using a throium - U^{235} standard slug.

V. NUCLEAR PHYSICS

A. Cross Sections Program

1. Crystal Spectrometer

a. Eta Measurements on U^{233} (J. R. Smith, E. H. Magleby)

The energy variation in eta for U^{233} is being measured on the MTR crystal spectrometer. A 120-gram sample of metallic U^{233} has been obtained on loan from England. The sample as mounted for the present experiment has an effective thickness to the beam of 6.9 g/cm^2. The experimental arrangement is the same as that previously used in determining the energy variation of eta for U^{235}. Fission neutron detectors are mounted beside the target at 90° to the beam. A single BF_3 counter behind the sample serves as both Bragg beam monitor and transmission detector as the sample is moved into and out of the beam by an automatic sample changer.

Originally the fission neutron detectors were both Hornyak buttons mounted on 5-inch photomultiplier tubes. One of these scintillation counters has been replaced by a "long counter" consisting of four BF_3 counters embedded in a cylinder of paraffin 7 inches in diameter and 10 inches long. A filter of B_4C 1/2-inch thick shields the long counter from slow neutrons elastically scattered from the sample. The long counter has a poorer signal-to-noise ratio than the Hornyak button, but its much

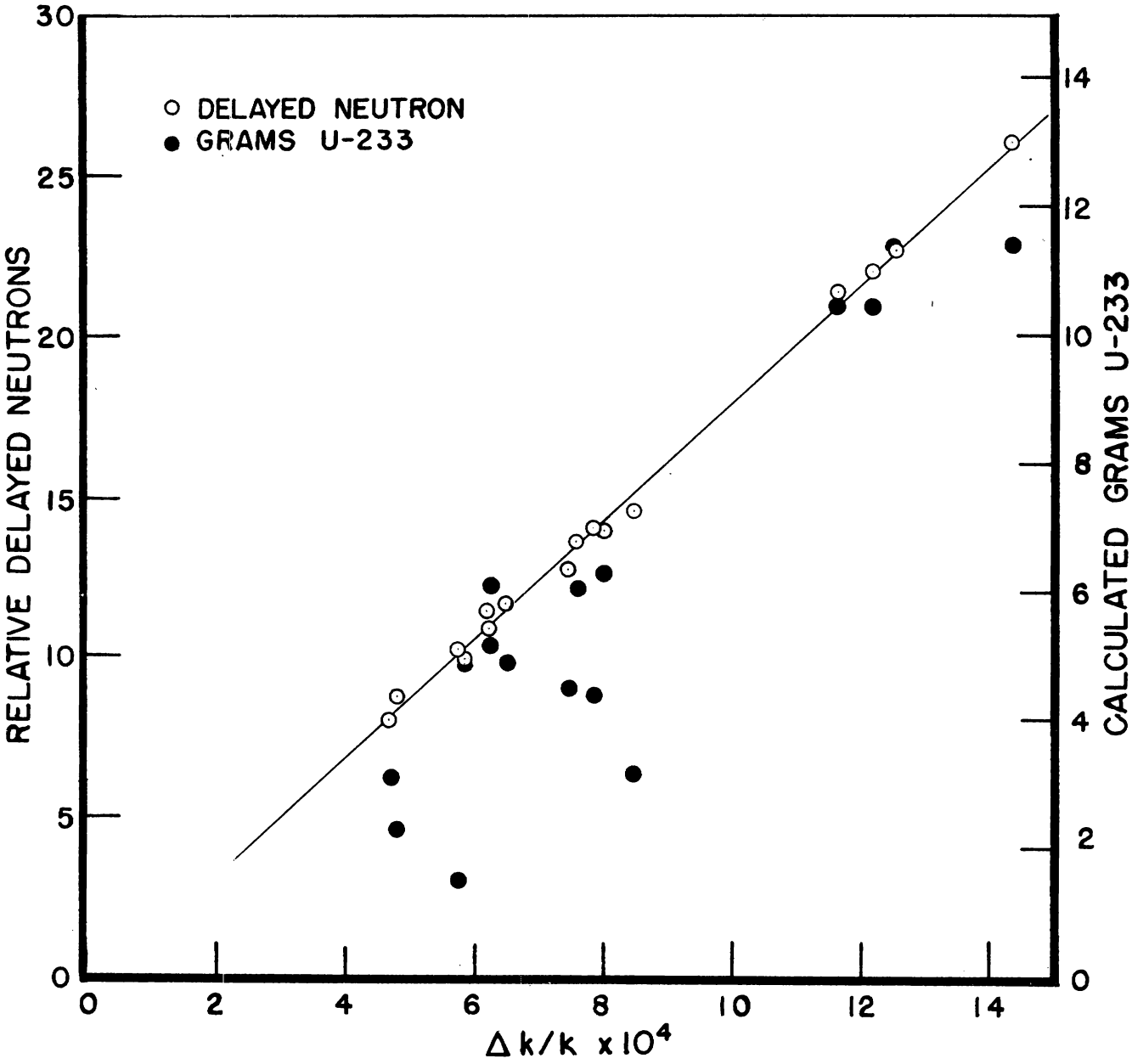

FIG. 9
DATA ON RD-I SLUGS

superior stability and efficiency more than compensate for this difficulty. It is anticipated that the second Hornyak button will also be replaced by a long counter in the near future.

The MTR data from 1 to 8 ev are shown in Figure 10, along with the Brookhaven data at lower energies. The solid line represents the fit to this data obtained by using the Wigner-Eisenbud multilevel formalism as discussed in the following section. Scattering corrections made on these data do not take into consideration loss of neutron energy in the scattering process. The effects of such energy losses are negligible except where the cross section is changing rapidly, as the steep sides of resonances. The solid line is calculated from resonance parameters determined from the fission cross section measurements made at MTR and the total cross section measurements of Brookhaven. Agreement between the two methods of determining eta is good. Order effects have not been removed from the MTR data. These, together with electronic and statistical fluctuations, may account for the dips in the regions of .15 and .7 ev. The most striking feature of the data is the sharp dip in eta at the 2.3 ev resonance. Other dips are evident corresponding to the higher energy resonances.

b. Resonance Parameters for U^{233} in the Energy Region below 4.0 ev
(M. S. Moore, C. W. Reich)

Recently, evidence has been discussed for the presence of interference between levels in slow neutron induced fission.[1,2,3] In particular, Sailor has fit the fission data for U^{235} in terms of a many-level formula. Bohr[3] has presented a model for the fission process based on the collective model which predicts interference between levels in fission.

The high resolution (0.09 μsec/meter) fission cross section data previously reported[4] have been extended to 4.0 ev, using the MTR crystal spectrometer. Attempts to fit these data using the single-level Breit-Wigner formula were not successful. The observed asymmetry of the levels indicated that interference was present.

In U^{233}, the level spacing is of the order of magnitude of the level widths for the first two resonances. As a consequence, the analysis the exact formulation of Wigner and Eisenbud[5] must be used.

---

1. V. L. Sailor, International Conference on the Peaceful Uses of Atomic Energy, Geneva, P/586 (1955).
2. J. A. Harvey and J. E. Sanders, Progress in Nuclear Energy, Ser. 1, 1, (1956).
3. Aage Bohr, International Conference on the Peaceful Uses of Atomic Energy, Geneva, P/911 (1955).
4. L. G. Miller and J. E. Evans, Bull. Am. Phys. Soc. 1, 247 (1956).
5. E. P. Wigner and L. Eisenbud, Phys. Rev. 72, 29 (1947).

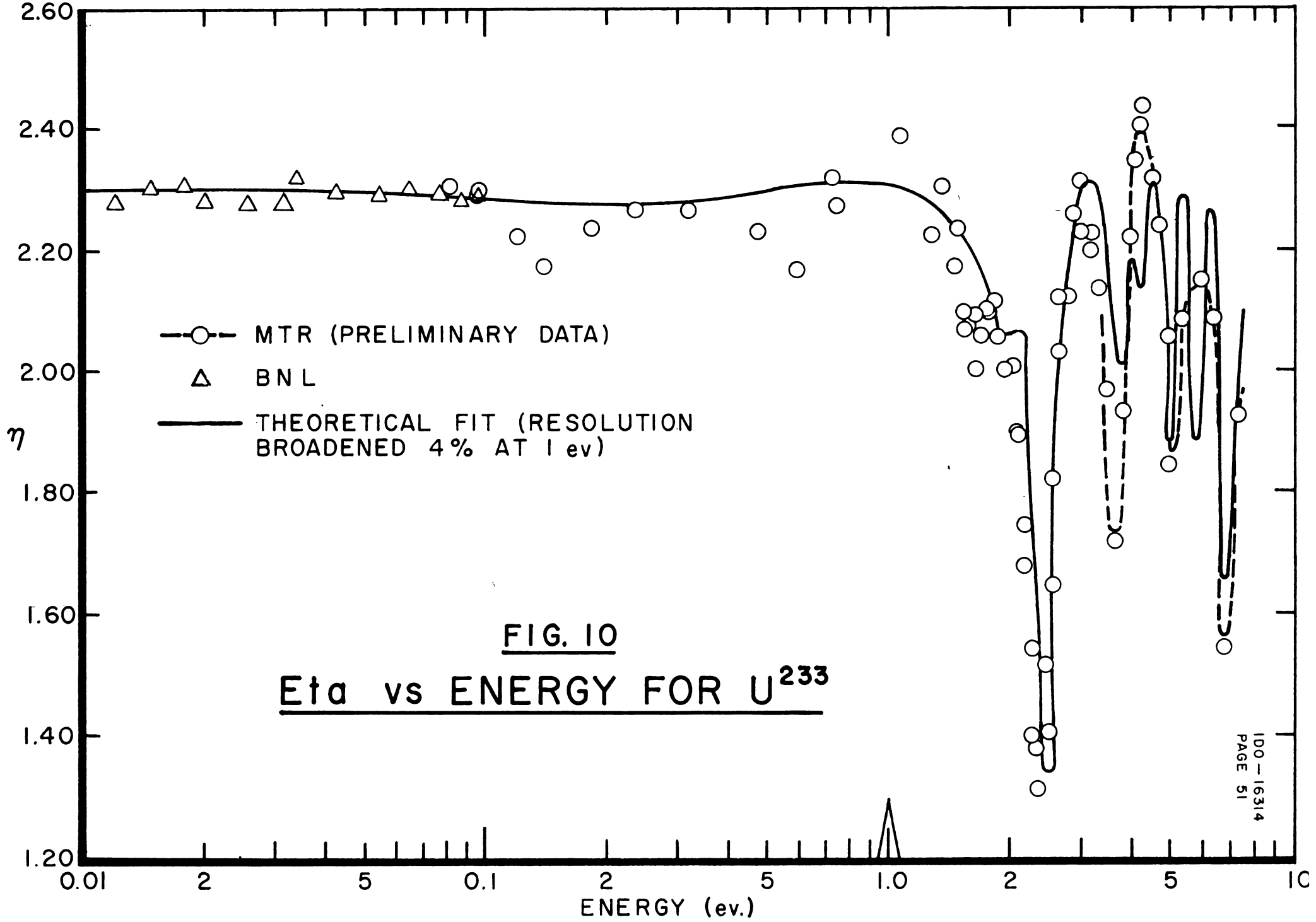

FIG. 10

Eta vs ENERGY FOR U^{233}

For $\ell = 0$ incident neutrons for a given spin state, and for a definite ℓ in the exit channel of the fission process, the cross section may be written as

$$\sigma_{nf} = g\pi \lambda_n^2 \left| S_{nf} \right| \qquad (1)$$

where S_{nf} is that element of the scattering matrix describing the fission process. The scattering matrix is related to the derivative matrix R, for $\ell = 0$ neutrons, by the expression

$$S = \omega \left(1 - i B R B\right)^{-1} \left(1 + i B R B\right) \omega$$

where the matrices B and ω are given by

$$B_{\alpha\beta} = \delta_{\alpha\beta} \sqrt{k_\alpha} \qquad \omega_{\alpha\beta} = \delta_{\alpha\beta} e^{i k_\alpha r_\alpha}$$

and for R the expansion is assumed

$$R_{\alpha\beta} = \sum_s \frac{\gamma_{\alpha s} \gamma_{\beta s}}{(E_s - E)} \qquad (2)$$

The $\gamma_{\alpha s}$ are for $\ell = 0$ neutrons related to the partial widths Γ_α^s by the expression

$$k_\alpha \gamma_{\alpha s}^2 = \Gamma_\alpha^s / 2$$

The analysis of the data thus requires an expression for S in terms of the parameters constituting R. Using the matrix identity

$$(1 - A)^{-1} (1 + A) = 1 + (1 - A)^{-1} 2A$$

one may write

$$\omega^{-1} S \omega^{-1} = 1 + 2 \left(1 - i B R B\right)^{-1} (i B R B)$$

For the case of fission in the presence of radiative capture, the simplest description is that of a three-channel process. These channels are elastic scattering, radiative capture, and fission. Additional channels would be required if one assumes that there may exist two or more modes of fission for the same resonance, or that there may be two or more outgoing orbital angular momentum values involved in fission. In the latter case, the

different terms for S_{nf} must be added coherently with the appropriate weighting factors, and the simple formula (1) no longer applies. If the simplest form is assumed, that of a three-channel multilevel process with full interference in fission, the equation, involving 3 by 3 matrices, can be solved. The element of the scattering matrix which describes fission has a leading term of the form

$$S_{nf} = e^{ik_n r_n}\left[\frac{2i\sqrt{k_n k_f}\, R_{nf}}{1 - i\sum_\gamma k_\gamma R_{\gamma\gamma}}\right] e^{ik_f r_f} \qquad (3)$$

The cross section can thus be written, correct to first order, as

$$\sigma_{nf} = \frac{4\pi g \lambda_n^2 k_n k_f \left(\sum_s \frac{\gamma_{ns}\,\gamma_{fs}}{(E - E_s)}\right)^2}{1 + \sum_{\nu\mu st}\left[k_\nu k_\mu \gamma_{\mu s}^2 \gamma_{\nu f}^2 / (E - E_s)(E - E_t)\right]} \qquad (4)$$

where μ and ν range over the channel values and s and t over the levels. Higher order terms are as a rule negligible. The first order expression, (4), is correct for four or more channels. In the case of a single level, the summation over s drops out and the formula reduces to the usual Breit-Wigner form.

The exact expression for the cross section, containing fourteen additional terms involving products of the derivative matrix elements $R_{\alpha\beta}$, has been programmed for a machine computation on the IBM 650. Cross Section as a function of energy is calculated for as many as fourteen interfering levels. Input data include the reduced width parameters γ_{ns} and $\sqrt{k_\nu}\,\gamma_{\nu s}$ and the resonance energies E_s. Provision has been made to include non-interfering components of the cross section and to correct the resulting curve for Doppler and resolution broadening.

Figure 11 shows the fit obtained to the U^{233} fission cross section data using the preliminary parameters listed below.

E_o(Exp)(ev)	-	1.785	2.30	3.63	-	4.5	4.7
E_o(Theory)(ev)	0.10	1.81	2.325	3.65	- 5.0	4.5	4.7
$g\Gamma_n^o(10^{-3}$ev)	1.67×10^{-3}	0.150	0.061	0.039	3.24	0.015	0.010
Γ_f (ev)	1.00	0.254	0.062	0.157	0.36	0.18	0.13
Γ_γ (ev)	0.040	0.045	0.040	0.040	0.041	0.040	0.040

The effects of resonances outside the 0-4 ev region are not necessarily unique. It is found that single-level parameters give a very good first approximation to the parameters to be used in the interference formula, especially if the levels are well separated. The energies of maximum cross section do not, however, correspond to the resonance energies as in the single-level case, but are displaced depending on the sign of the interference term.

FIG. 11

U^{233} FISSION CROSS SECTION

(THEORETICAL FIT HAS BEEN DOPPLER BROADENED)

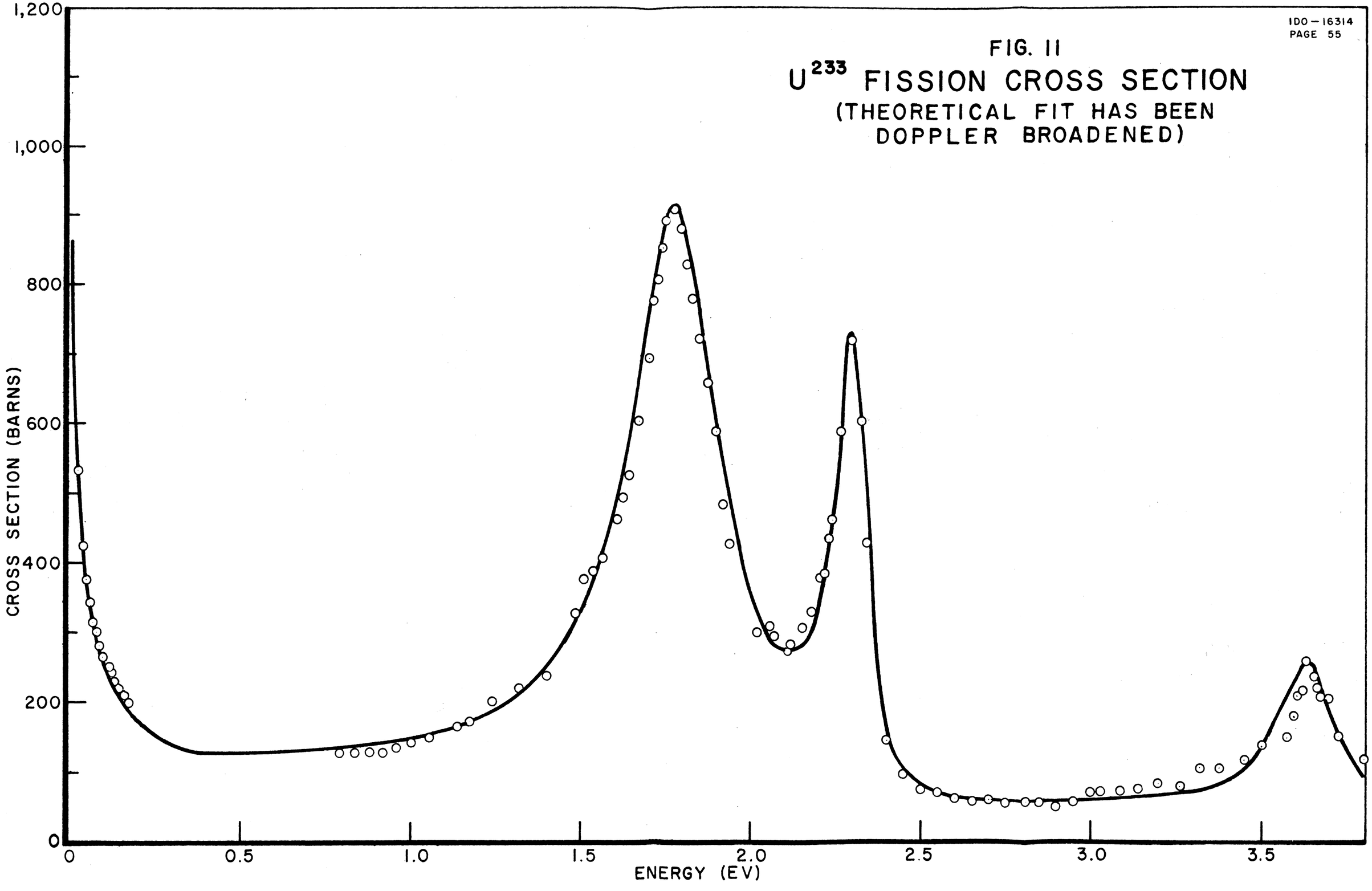

The sign of the interference term can be determined uniquely by a direct measurement of eta, the number of neutrons emitted per neutron absorbed in fission, as a function of energy. Eta contains, as the single energy dependent variable, the radiative capture to fission ratio. The radiative capture process is not expected to show interference, since it has a large number of exit channels available. Thus, if the curve of eta vs. energy has a slope at the resonance energy, interference is indicated, and the sign of the interference term is given by the slope at that point. Figure 10 shows a plot of eta as a function of energy for U^{233}. The experimental points above 0.1 ev have been taken with the MTR crystal spectrometer as reported in the preceding section. The theoretical fit is seen to be excellent.

c. Fission Cross Section Measurements (Crystal Spectrometer) (L. G. Miller)

A fission chamber capable of supporting 40 fission foils has been constructed. The foils will be divided into about 8 groups, each group having an independent amplifier in order to reduce the alpha pile-up problem. The chamber is being assembled with U^{233} foils for the purpose of improving statistics on the high resolution fission cross section measurements. With the new chamber, it is planned to extend the crystal spectrometer data to 10 ev.

d. High Resolution Collimator (Crystal Spectrometer) (L. G. Miller, J. R. Smith)

A pilot model of a new type high resolution collimator has been assembled. This collimator uses foils of polyethylene to form 0.010-inch wide collimating channels. Advantages of polyethylene are that it is easy to stretch and it will eliminate total reflection in the collimator. Furthermore, the radiation hazards from (η, γ) reactions in the collimator will be greatly diminished.

2. Fast Chopper

a. Fission Cross Section of U^{233} (Fast Chopper) (L. G. Miller, R. G. Fluharty, R. M. Brugger)

Measurements of the fission cross section of U^{233} have been made on the fast chopper from 1.1 to 13 ev and are being extended to higher energies. Two fission chambers with six 5-inch diameter coated foils (0.5 mg/cm^2 of U^{233} oxide) in each chamber, are being used with one μsec channels and a 16 meter flight path. Each foil has its own wide band preamplifier. Signals from the first chamber are delayed by an amount equal to the mean neutron flight-time between the two chambers.

Figure 12 is a plot of the preliminary data. The arrows indicate the position of resonances reported in the total cross section. The overall agreement with MTR high resolution crystal spectrometer is very good. There are some differences in details which need to be clarified.

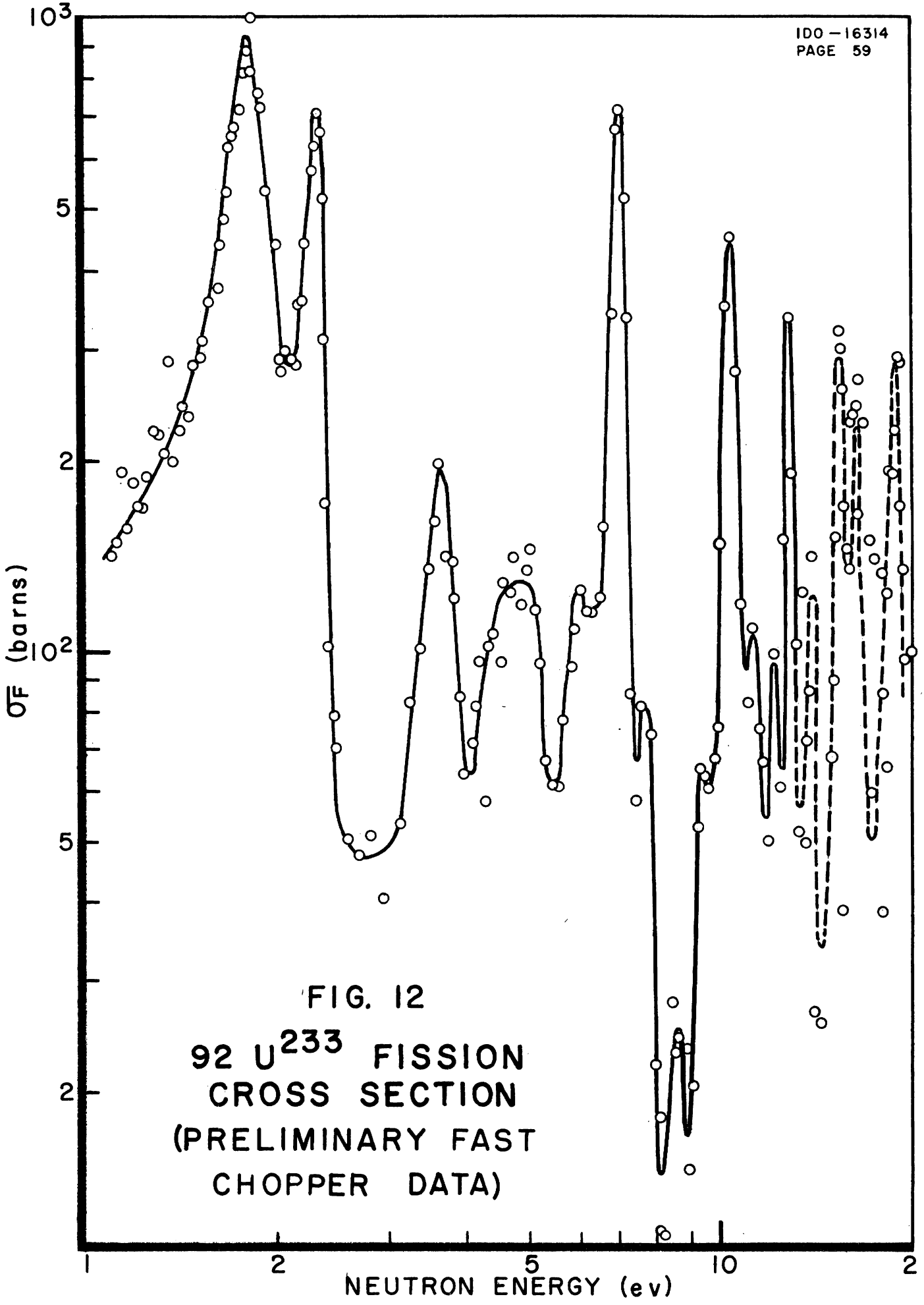

FIG. 12

92 U^{233} FISSION CROSS SECTION (PRELIMINARY FAST CHOPPER DATA)

b. 1024 Channel Analyzer (F. L. Petree)

1) Control Circuits

The MTR 1024 channel analyzer control circuits are shown block-diagramwise in Figure 13. The 4 mc pulsed L-C oscillator, a Brookhaven design, eliminates the quarter-microsecond jitter that occurs in gated crystal oscillators, while increasing the possibility of objectionable drift. Temperature regulation will be employed, if necessary, on critical components.

The frequency divider provides channel width adjustment, by factors of two, from 1/4 to 16 microseconds. The leftmost flip-flop eliminates gating uncertainties by delaying storage of a detected pulse until the next pulse receives from the frequency divider. This has the effect of increasing the average dead time by 1/2 the channel width. An effort will be made to eliminate this dead time in the 16 microsecond channel width where it will be the most objectionable.

The detector pulse shaper generates a negative gating pulse during the 16 microsecond storage interval. It is a pulsed cathode follower, as shown in Figure 14. This circuit has a much faster rise time than an ordianary flip-flop circuit, and was a major factor in allowing operation at quarter-microsecond channel widths. Another factor was the incorporation of a threshold trigger circuit after the leftmost gate in Figure 13.

The adjustable time delay before storage is generated by the ten flip-flop elements in the address scaler, plus the two time delay tubes, to provide a total delay of 4096 channels. During the delay period the detector gates are held shut by the rightmost flip-flop. As explained in the last quarterly report, the delay can be reduced by switching a set-up delay pulse so that it flips appropriate address or delay flip-flops after the display interval.

The quadrant selector switch has nine positions and controls the last two flip-flops of the address scaler. The following list illustrates the 9 modes of operation of the analyzer which are determined by the quadrant selector switch.

QUADRANT SELECTOR SWITCH

Switch Position	Channels of Storage	Quadrants
1	1024	1,2,3,4
2	512	1,2
3	512	3,4
4	512	Detector Controlled
5	256	1
6	256	2
7	256	3
8	256	4
9	256	Detector Controlled

FIG. 13

1024 CHANNEL ANALYZER CONTROL CIRCUIT

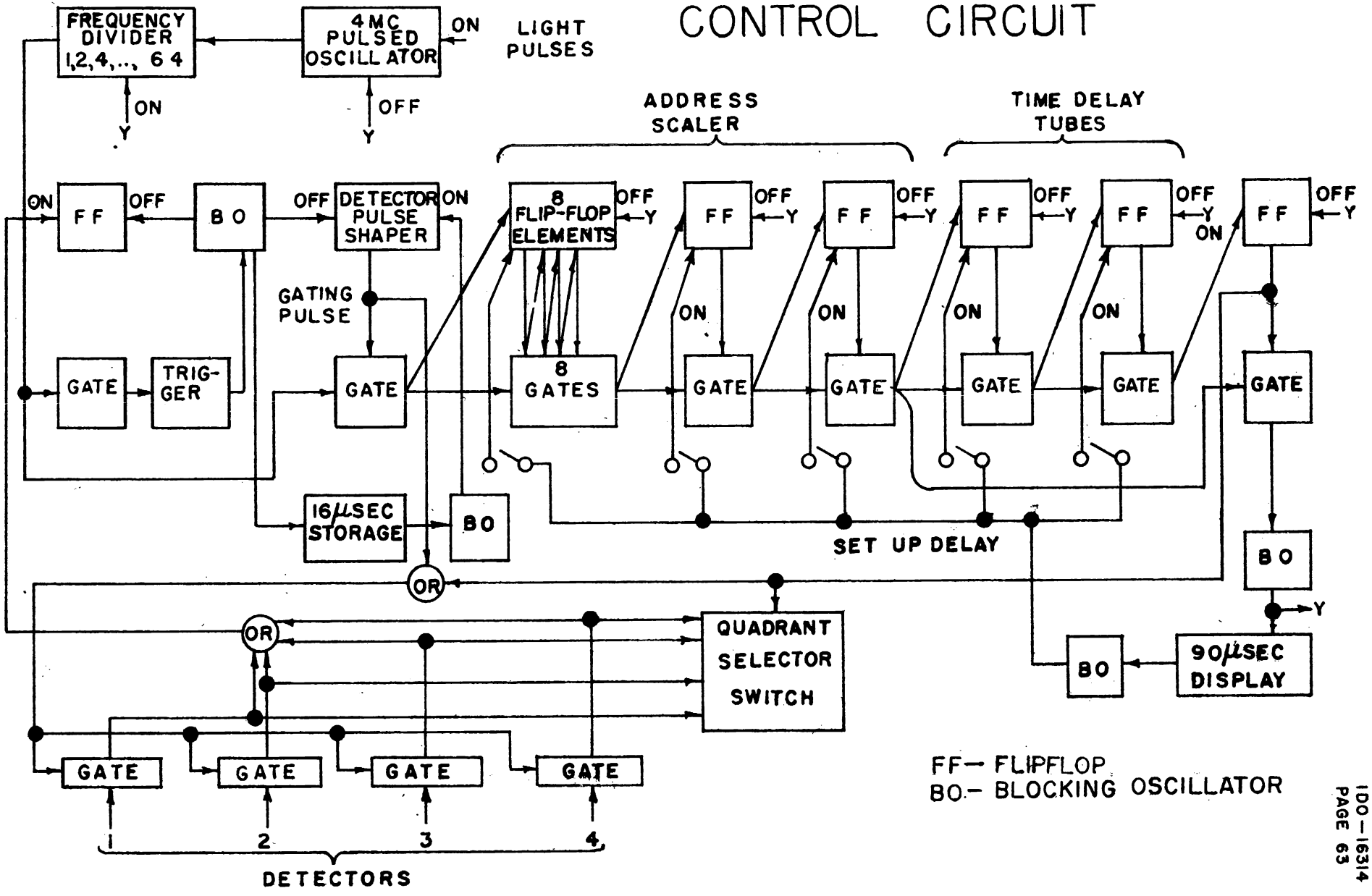

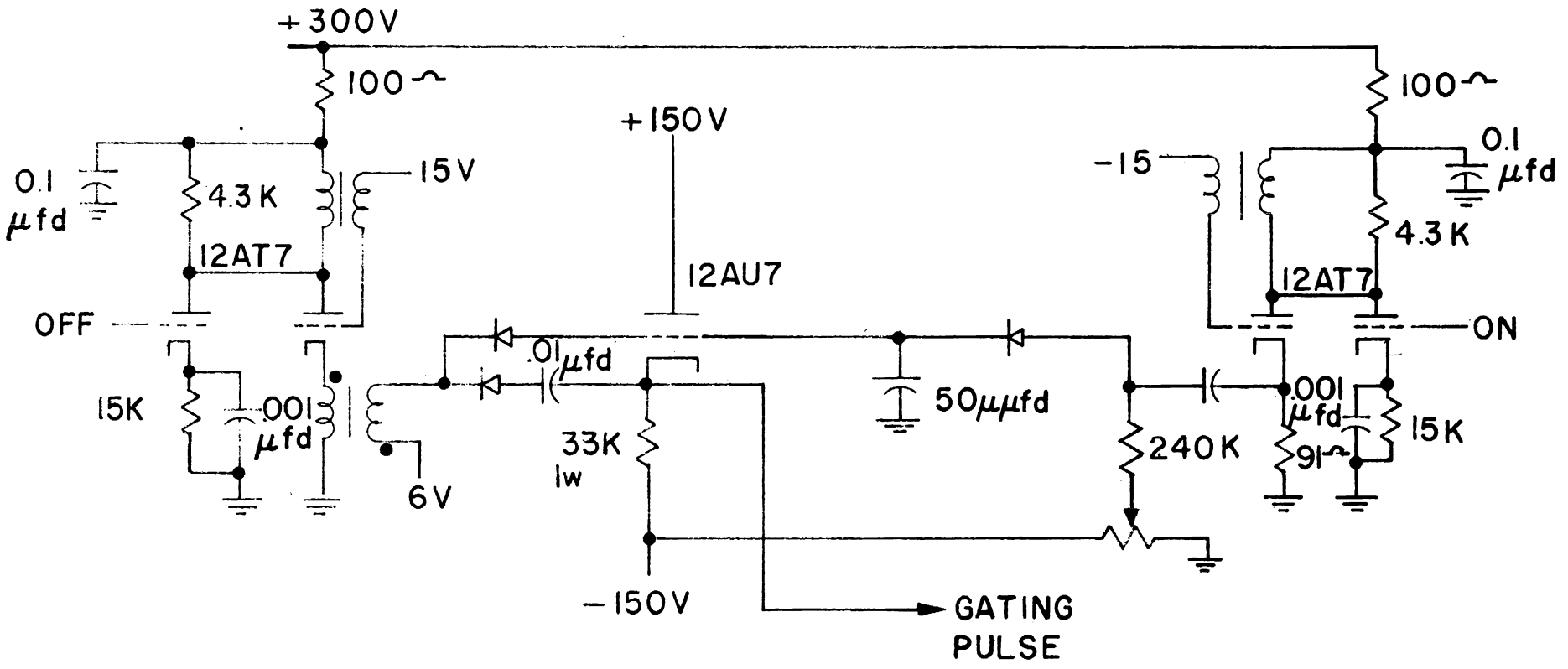

FIG. 14

DETECTOR PULSE SHAPER CIRCUIT

2) Printout System

Some modification of the display system was made to allow it to be re-used during the period of recording the information accumulated in the cores during a run. Accordingly, Figure 15 is a revision of Figure 32 from page 117 of IDO-16297. The display system functions nearly the same as before.

For recording, the 50 microsecond monostable multivibrator is caused to become astable with an adjustable period of approximately one second. When a print control flip-flop is triggered, the astable multivibrator begins cycling and a relay closes to start a recorder. The reset blocking oscillator is disabled so that the address advances once each cycle. The addressed cores are read and the display on a pen recorder appears as a continuous histogram.

Selection of particular quadrants for printout is made by means of the quadrant selector switch.

3. Inelastic Scattering of Slow Neutrons (R. M. Brugger)

The conceptual design for a collimating plug for the HG-6 facility of the MTR has been completed. Some of the design features are: (1) 2-inch by 4-inch maximum beam size, (2) a combination internal beam cut-off and variable width collimator, and, (3) vacuum tight seals so the beam path can be evacuated when working with very cold neutrons.

A study has been made of the intensities, resolution, and applicable energy ranges to be expected from the different instrumental arrangements which can provide the monenergetic neutrons for the measurement of angular and energy distributions of the scattered neutrons. A very versatile high counting rate system consists of two Fermi-type choppers separated in distance along the beam path, and operated with a fixed phase difference. This is a modification of the system being developed by Egelstaff at Harwell and provides counting rates of the same order of magnitude. The new systems, which will provide an order of magnitude increase in the calculated intensities in an experiment which was previously borderline, became possible when it appeared feasible to phase high speed chopper rotors. The gain in intensity results from the low beam collimation permitted by these systems. Another gain in intensity is made possible by having bursts of monoenergetic neutrons hitting the scattering sample. This situation permits the simultaneous accumulation of data for the neutrons scattered at several different angles.

Journal Publications

1) "The Total Neutron Cross Section of Thulium in Energy Region 0.038 to 1.56 ev", E. G. Joki and J. E. Evans (Published in Phys. Rev. 103, 1326, September 1, 1956).

2) "Neutron Resonance Measurements of Ag, Ta, and U^{238}", R. G. Fluharty, F. B. Simpson, and O. D. Simpson. (Published in Phys. Rev. 103, 1778, September 15, 1956).

3) "Neutron Resonance Parameters and Transmission Measurements in U^{235}", O. D. Simpson, R. G. Fluharty, and F. B. Simpson. (Published in Phys. Rev. 103, 971, August 15, 1956).

4) "The Total Neutron Cross Section of Chlorine and Carbon", R. M. Brugger, J. E. Evans, E. G. Joki, and R. S. Shankland. (To be published in Phys. Rev. - November 15, 1956).

B. Decay Schemes and Nuclear Isomerism

1. Decay of 11 hr Y^{93} (R. L. Heath)

The decay of fission produced Y^{93} has been studied using scintillation spectrometry. This study has included gamma ray energy and intensity measurements, beta ray transitions, and coincidence relationships from which a tentative decay scheme can be constructed.

Samples of Y fission product activity were prepared by irradiation of uranium samples in a high flux facility of the MTR. A chemical separation of the yttrium fraction was then made from gross fission products as rapidly as possible to achieve a maximum ratio of Y^{93} to Y^{92} and Y^{91} activities. A suitable decay period was then allowed to remove the remaining short-lived contaminants.

Gamma Radiation: The gamma radiation emitted was investigated with the MTR 100-channel gamma spectrometer using a 3-inch by 3-inch NaI detector. The pulse spectrum obtained indicated the presence of several gamma rays which decayed with a measured half life of 11.0 ± 0.4 hr. The gamma spectrum was analyzed to obtain the relative intensity of each gamma ray. To permit this analysis it was necessary to remove the contribution from bremsstrahlung produced in the absorption of the 3.1 Mev ground-state beta transition which accounts for 85 percent of the decay of 64 hr. Y^{90} (2.3 Mev) was used as a model and fitted to the high-energy end of the Y^{93} gamma ray spectrum. A summary of the gamma ray spectrum is shown below:

TABLE X

Gamma Ray	Gamma Energy (Mev)	Relative Intensity
γ_1	0.265 ± 0.005	1.000
γ_2	0.455 ± 0.008	0.034 ± 0.006
γ_3	0.675 ± 0.01	0.151 ± 0.015
γ_4	0.940 ± 0.01	0.366 ± 0.037
γ_5	1.15 ± 0.02	0.053 ± 0.01
γ_6	1.40 ± 0.02	0.097 ± 0.015
γ_7	1.88 ± 0.02	2.232 ± 0.023
γ_8	2.14 ± 0.02	0.085 ± 0.01

The gamma spectrum of 11 hr. Y^{93} is shown in Figure 16.

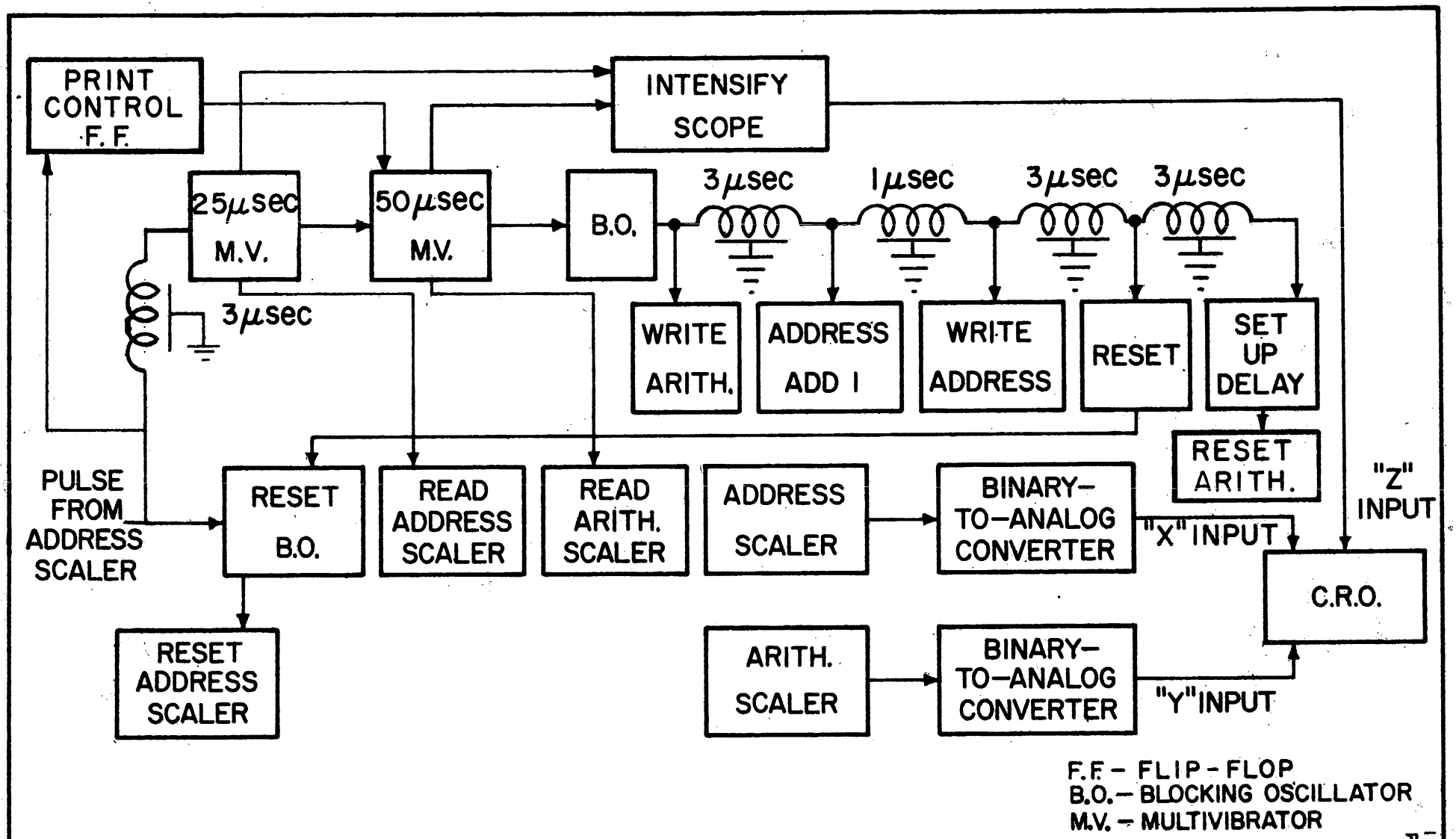

FIG. 15

BLOCK DIAGRAM OF DISPLAY SYSTEM

FIG. 16

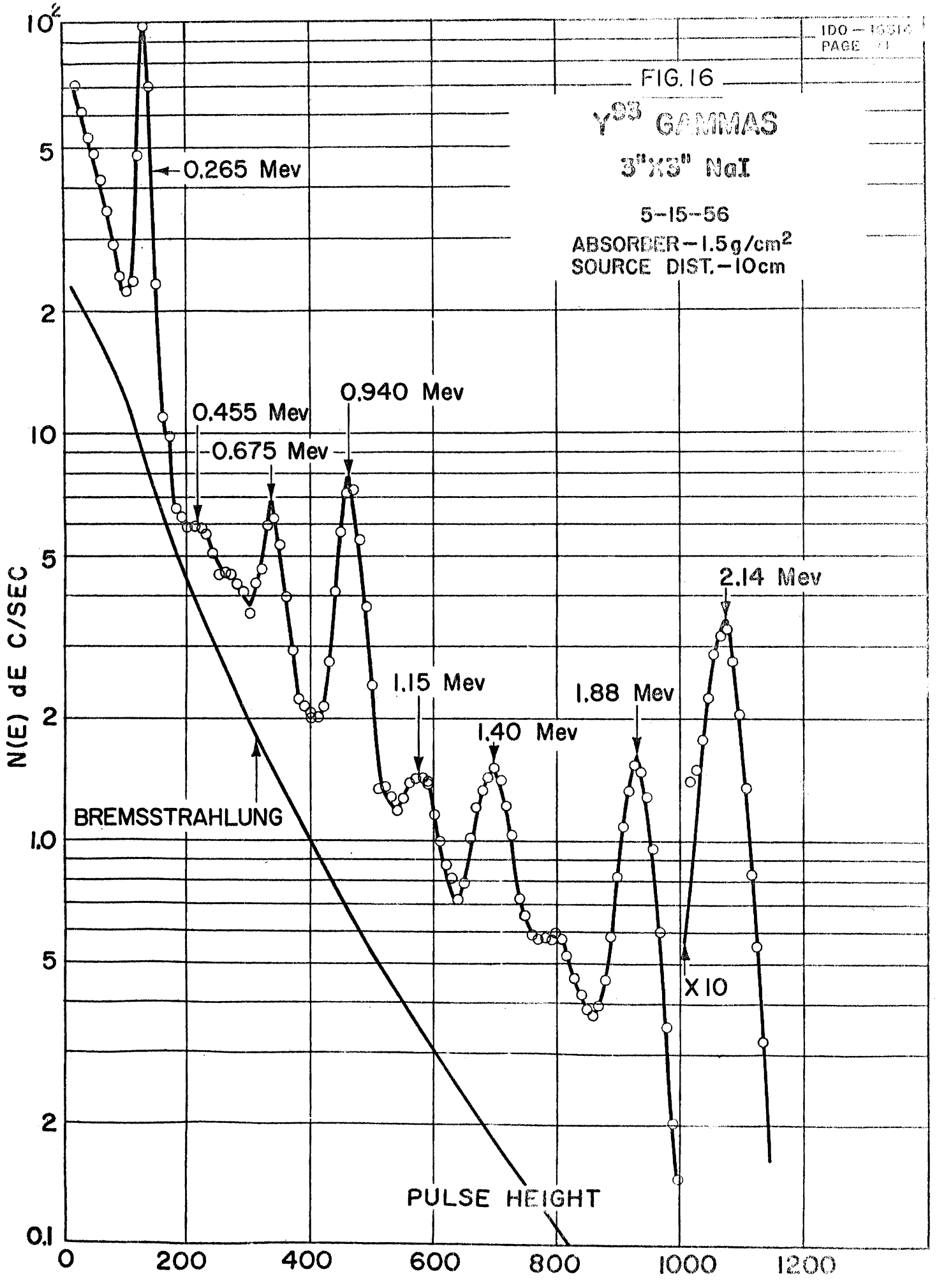
Y^{93} GAMMAS
3"X3" NaI
5-15-56
ABSORBER – 1.5 g/cm²
SOURCE DIST. – 10 cm
0.265 Mev
0.455 Mev
0.675 Mev
0.940 Mev
1.15 Mev
1.40 Mev
1.88 Mev
2.14 Mev
BREMSSTRAHLUNG
PULSE HEIGHT
X 10
N(E) dE C/SEC
10²
5
2
10
5
2
1.0
5
2
0.1
0
200
400
600
800
1000
1200

γ-γ Coincidence Studies: Gamma-gamma coincidence spectra were obtained using two 2-inch by 2-inch NaI detectors mounted with their axes in a horizontal line with a spacing of 4.0 cm between crystal faces. A graded backscatter shield was inserted to reduce false coincidence effects from scattering between the two detectors. Polystyrene absorbers were used to stop beta radiation. The coincidence circuit used was of the "fast-slow" type to permit pulse-height analysis. The system was operated with a resolving time of 0.5×10^{-6} sec. A sliding-window single-channel analyzer was operated in coincidence with the 100-channel spectrometer so as to obtain the spectrum of radiation coincident with a particular energy region selected with the single-channel machine. In this manner it was possible to determine many of the coincidence relationships between the different gamma rays emitted in the decay of this nuclide. A summary of the confirmed relationships is shown in Table XI.

TABLE XI

Gamma-Gamma Coincidence Relationships

Gamma Ray Energy (Mev)	Coincident with (Mev)
0.265	0.675, 1.15, 1.88, 0.455
1.88	0.265
2.14	None

Decay Scheme: Interpretation of the gamma ray energy spectrum and the coincidence measurements made it possible to propose a tentative decay scheme which is consistent with the observed experimental data. In order to determine the beta ray branching ratio to the excited states of the daughter nucleus a comparison was made between the absolute beta emission rate and the emission rate for each gamma ray. Sources of the fission product Y fraction were prepared for counting in a 4-pi flow proportional chamber. The decay of these samples was followed for a sufficient time to permit the subtraction of the contributions from 3.5 hr. Y^{93} and 54 day Y^{91}, present as minor contaminants. The disintegration rate thus obtained was then compared with the emission rate for the gamma rays obtained by measurement of the gamma ray spectrum with 3-inch by 3-inch NaI detector. On the basis of this comparison the 3.1 Mev beta transition to the ground state was found to account for 85 percent of the transitions. Utilizing the gamma ray energy data together with the determined coincidence relationships it was possible to deduce the end-point energy and relative intensity of the major beta ray groups leading to excited states of the daughter nucleus. These are listed in Table XII below:

TABLE XII

Intensities of the β-ray transitions computed from γ-ray data
(transitions labeled by final state)

Beta ray Group	Intensity
$\beta 0$	0.85
$\beta 0.265$	0.055
$\beta 0.940$	0.047
$\beta 1.40$	0.018
$\beta 2.14$	0.031

The tentative decay scheme proposed, constructed from the experimental data discussed above, is shown in Figure 17. The origin of the 0.94, 1.40, and 2.14 Mev gamma rays is derived from a negative result in the coincidence studies. The assignment of the origin of the 0.455 and 1.15 Mev gamma transitions is based largely on energy considerations. More extensive coincidence measurements including β-γ determinations are planned to substantiate this decay scheme.

2. Scintillation Detector Efficiency Calculation (S. H. Vegors)

A very basic problem in the use of a scintillation counter as a precision instrument in gamma ray spectroscopy is the calibration of the NaI(Tl) crystal. In particular, if one detects N events/sec with a counter it is desired to know the number, No, of radioactive decays/sec in the source for a given source-detector configuration. A calculation of this ratio, N/No, has been undertaken on the IBM 650 for two different types of sources. In the first case a point source of radiation is located a distance h along the extended axis from the near face of a right circular NaI(Tl) crystal whose radius is r and whose thickness is t. Calculations are being made for 15 values of h ranging from 0 to ∞, for 14 different gamma ray energies ranging from 8.9 Kev (γ = 600 cm^{-1}) to 7.4 Mev (γ = 0.123 cm^{-1}, and for 32 crystal sizes ranging from 1-inch by 1/16-inch to 1-1/2-inch by 6-5/8-inch.

The second case is for a disk source of radioactivity of radius R mounted with its plane perpendicular to the axis of a right circular cylindrical NaI(Tl) crystal of radius r and thickness t and at a distance h above the near face of the crystal. For this case each calculation is much more difficult and requires more computor time. However, it is anticipated that calculations will be made for at least values of R = 1/2r, 3/4r, and r for 3-inch by 3-inch and 1-3/4-inch by 2-inch crystals.

C. Cross Section of Tm^{170} for Pile Neutrons (S. D. Reeder, E. H. Turk)

In the production of thulium x-ray sources at the MTR, thulium metal is irradiated with neutrons to produce Tm^{170} by the reaction Tm^{169} (n,γ) Tm^{170}. The Tm^{170} is a radioactive nuclide which decays with a half life of 129 days emitting an 84 Kevγ which is highly converted producing a 55 Kev x-ray. The Tm^{170} can undergo further neutron capture by the process Tm^{170} (n,γ) Tm^{171}. The Tm^{171} is a beta emitter only and would decrease the source strength of the thulium metal if it were allowed to build up. The cross section of this second reaction is not known precisely. It has been estimated, from nuclear systematics, to be of the order of thousands of barns. Some very preliminary work also suggested a value of about 1000 barns. Since the value of the Tm^{170} cross section is important for calculating the irradiation time to produce the maximum amount of Tm^{170}, a program was undertaken to measure this quantity.

A solution of Tm metal in 3N nitric acid was prepared from specially purified Tm metal received from Dr. Spedding of the Ames Laboratory. Three identical samples were prepared containing 0.1 μg Tm in solution. These samples were encapsulated in quartz ampoules which were irradiated in "leaky rabbits" in L-45 position in the MTR. The irradiation history is shown in Table XIII. The nvt therein listed was measured by means of an

FIG. 17
DECAY SCHEME
OF
11.2 hr Y^{93}

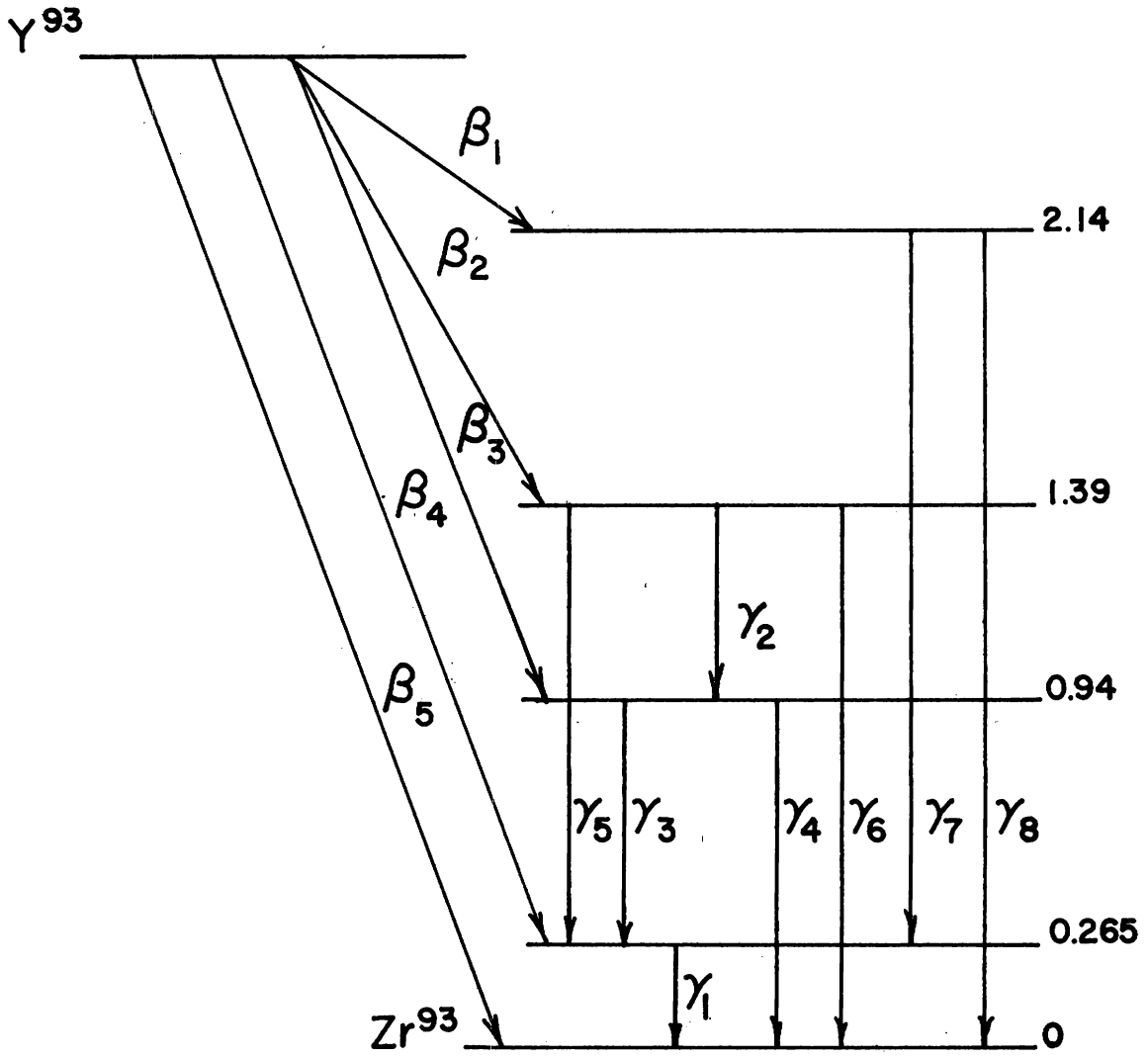

aluminum-cobalt alloy monitor. The irradiation was carried out over three consecutive cycles with one sample being removed after each cycle. This gave samples with one, two and three cycles of irradiation.

The samples were all allowed to decay until the last sample out of the reactor had cooled for approximately 30 days. The capsules were then opened and the solution transferred quantitatively to a 10.0 ml volumetric flask using 3N nitric acid. Measured aliquots of these samples were mounted on teflon and the activity measured both on a gamma scintillation spectrometer and a proportional counter. The gamma spectra of the Tm activity showed only the presence of Tm^{170} activity. The relative activity of the samples agreed for both the gamma peaks from the spectrometer and total beta counts obtained with the proportional counter. These data are given in Table XIV.

The data in Table XIV were used with the production equation for Tm^{170} based on the overall reaction:

$$Tm^{169} \xrightarrow[\sigma = 129 \text{ Barns}]{(n,\gamma)} Tm^{170} \xrightarrow[\sigma_1 = ?]{(n,\gamma)} Tm^{171} \qquad (1)$$

$$Tm^{170} \xrightarrow{\beta} Yb^{170} \text{ (stable)}$$

$$T_{\frac{1}{2}} = 127 \text{ days}$$

The final form of the production equation is

$$A = \frac{\sigma_o \phi}{\sigma_1 \phi + \lambda - \sigma_o \phi} \left[e^{-\sigma_o \phi t} - e^{-(\sigma_1 \phi + \lambda) t} \right] \qquad (2)$$

where

σ_o = Cross section for Tm^{169} neutron capture

σ_1 = Cross section for Tm^{170} neutron capture

ϕ = Neutron flux

t = Irradiation time (seconds)

λ = Decay constant for Tm^{170}

TABLE XIII

Irradiation of Tm for Measurement of Tm^{170} Pile Neutron Cross Section

Sample in L-45 Position in the MTR

Irradiation	nvt (x 10^{-20})	MWD
MTR Cycle 69	7.0	605
MTR Cycles 69 & 70	15.0	1216
MTR Cycles 69, 70 & 71	25.3	1980

TABLE XIV

Relative Tm^{170} Activity Produced with Neutron Irradiation

Irradiation	Normalized Activity *	
(nvt x 10^{-20})	Prop. Counter	Scint. Counter
7.0	1.00	1.00
15.0	1.79	1.81
25.3	2.51	2.50

* Corrected for decay to end of irradiation in reactor.

Selected values of σ_1 were inserted into equation (2) until the calculated activity agreed with the observed value. A value of 150 barns for σ_1 gave the best fit to the data.

RECEIVED
PHILLIPS PETROLEUM CO.
JAN 3 1957
NRTS
TECHNICAL LIBRARY

Phillips 66